ESD-TR-91-174

Technical Report
940

Maximum Likelihood Detection of Electro-optic Moving Targets

S.C. Pohlig

16 January 1992

Lincoln Laboratory
MASSACHUSETTS INSTITUTE OF TECHNOLOGY
LEXINGTON, MASSACHUSETTS

Prepared for the Department of the Air Force under Contract F19628-90-C-0002.

This report is based on studies performed at Lincoln Laboratory, a center for research operated by Massachusetts Institute of Technology. The work was sponsored in part by the Space Systems Division, Department of the Air Force under Contract F19628-90-C-0002.

The ESD Public Affairs Office has reviewed this report, and it is releasable to the National Technical Information Service, where it will be available to the general public, including foreign nationals.

FOR THE COMMANDER

Hugh L. Southall

Hugh L. Southall, Lt. Col., USAF
Chief, ESD Lincoln Laboratory Project Office

MASSACHUSETTS INSTITUTE OF TECHNOLOGY
LINCOLN LABORATORY

MAXIMUM LIKELIHOOD DETECTION OF ELECTRO-OPTIC MOVING TARGETS

S.C. POHLIG
Group 27

TECHNICAL REPORT 940

16 JANUARY 1992

LEXINGTON MASSACHUSETTS

EXECUTIVE SUMMARY

Maximum Likelihood Detection Algorithm

The description of a maximum likelihood algorithm to detect moving targets in electro-optic data is presented. The algorithm is evaluated in terms of the probabilities of false alarm and detection. A comparison of theoretical and experimental probability distributions for single normalized pixels shows good agreement. Similarly, a comparison of theoretical and experimental false alarm probabilities also shows good agreement. These results validate using theoretical models to predict algorithm performance. Several detection examples are shown.

The data sets compared against theory are obtained from different sensor types, wavebands, and clutter backgrounds. The Experimental Test System sensor provides visible band data from a staring sensor. The background clutter in these data sets consists of stars and other deep space objects. The Infrared Measurements Sensor (IRMS) provides long and medium wavelength infrared data from a scanning sensor. Background clutter in the IRMS data sets consists of sky, mountains, hills, and desert.

Binary Integration Algorithm and Architecture

A binary integration version of this algorithm is described and evaluated in terms of false alarm and detection probabilities. This version is suboptimum and is compared with the optimum algorithm to determine the performance loss. A processing architecture concept is also described.

Conclusion

The model used in the maximum likelihood algorithm development is shown to closely agree with experimental data when the clutter background has temporally stationary statistics. An accurate model allows the algorithm performance (probabilities of detection and false alarm) to be precisely predicted. Potential areas for future work include: (1) development of processing architectures and efficient algorithm implementations for fast computation, (2) inclusion of target signal (signal-to-noise ratio) statistics in the model to investigate improved algorithms, and (3) investigation of frame registration issues and techniques.

Maximum Likelihood Algorithm Derivation

An algorithm to detect moving targets in electro-optic data is derived for the case where the data samples have Gaussian (normal) distributions that are temporally stationary (frame to frame) and spatially nonstationary (pixel to pixel). In other words, the means and variances describing the data samples are assumed to vary among pixels according to the background scene but remain constant over time. Additionally, these underlying means and variances are presumed unknown. Targets are assumed to have an arbitrary distribution.

Single Pixel Probability Distributions

The probability distribution of a single normalized pixel (used in the likelihood function) is derived. This distribution is used elsewhere to derive the theoretical probabilities of false alarm and detection.

In the case of noise-only (no target), the probability distribution is shown to be an instance of a beta distribution. With a target present, the probability distribution is a noncentral beta distribution. These distributions depend on the background clutter scene only through the noncentrality parameter, which is proportional to the signal-to-noise ratio.

Likelihood Function Statistics

The probabilities of false alarm and detection are derived for the maximum likelihood detection algorithm. Evaluation of these probabilities is accomplished through numerical integration.

ACKNOWLEDGMENTS

Various colleagues at Lincoln Laboratory have helped in the development of the work discussed in this report. Anthony E. Filip and Gary A. Shaw provided valuable technical interaction. Joaquin J. Otazo and John J. Tremblay provided details on the IR data and data collection. Chris T. Sung assisted with the software and processing of data files. Albert H. Huntoon suggested the method of placing velocity filters in parallel for the binary detection algorithm.

TABLE OF CONTENTS

LIST OF ILLUSTRATIONS

LIST OF TABLES

1. MAXIMUM LIKELIHOOD DETECTION ALGORITHM

An algorithm to detect moving targets in electro-optic data is developed and analyzed. In such data moving targets are distinguished by their motion relative to a fixed background scene (clutter). Unresolved targets may appear as a "streak" in a single image frame collected with a staring sensor or as a dot in a single image frame from a scanning sensor. A sequence of images can be used to distinguish between clutter and targets.

A maximum likelihood algorithm is derived to detect a target with an arbitrary signal distribution against unknown clutter. A consequence of this algorithm is that detection thresholds may be set according to a given false alarm rate without knowledge of the background clutter scene. Experimental false alarm performance is compared against the theoretical predictions and found to closely agree.

The data used to test this algorithm are obtained from two sensors developed at Lincoln Laboratory. The Experimental Test System (ETS) sensor is a visible band staring sensor that is ground-based and typically used to detect moving objects against a nighttime stellar background. In these data clutter consists of stars and other deep space objects as well as atmospheric effects, notably clouds. Figure 1 shows an unprocessed image from the visible band test data sequence. A pseudocolor mapping indicates intensity.

The Infrared Measurements Sensor (IRMS) is a scanning sensor that collects both long wavelength infrared (LWIR, 8 to 12 μm) and medium wavelength infrared (MWIR, 3 to 5 μm) data. This sensor is typically used with a clutter background of sky, mountains, desert, and forest. Both sensor types work well with this algorithm. Figures 2 and 3 show unprocessed images from three of the IR test data sequences. Again, a pseudocolor mapping indicates intensity.

The technical discussion that follows is divided into four parts. A statement of the maximum likelihood detection algorithm is given first. The theoretical probability distribution of normalized data is second with a comparison of the theoretical and experimental results. The theoretical probability of false alarm and false alarm rate are third, also with a comparison of the theoretical and experimental results. The final section presents the theoretical detection probability and includes several detection examples.

1.1 Signal Model and Algorithm

The maximum likelihood moving target detection algorithm is derived under the assumption that data samples collected from a sequence of image frames are independent, normally (i.e., Gaussian) distributed random variables. In the absence of targets, these samples are modeled as stationary in time but nonstationary in space. In other words, the means and variances of the data samples are assumed to vary from pixel to pixel, but for a single pixel they are constant over time.

The motivation for an independent normal statistics model is based on assumptions of (1) independent thermal and readout sensor noise and (2) independent arrival of photons to each

Figure 1. Single unprocessed frame of ETS Magellan data.

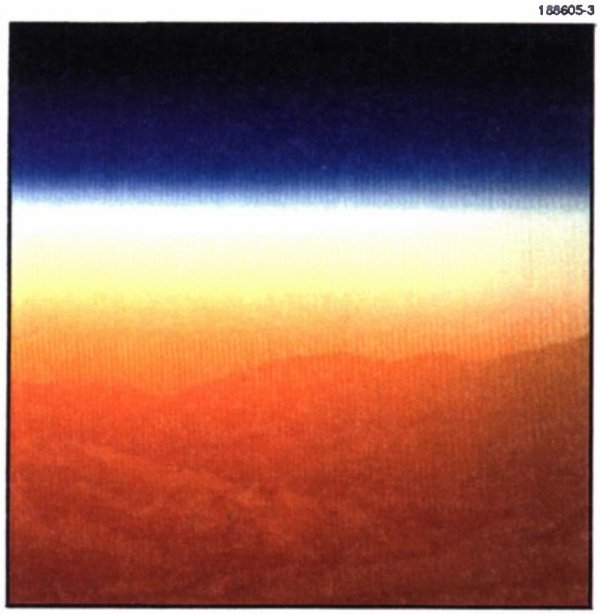

Figure 2. Single unprocessed frame of IRMS Longjump data.

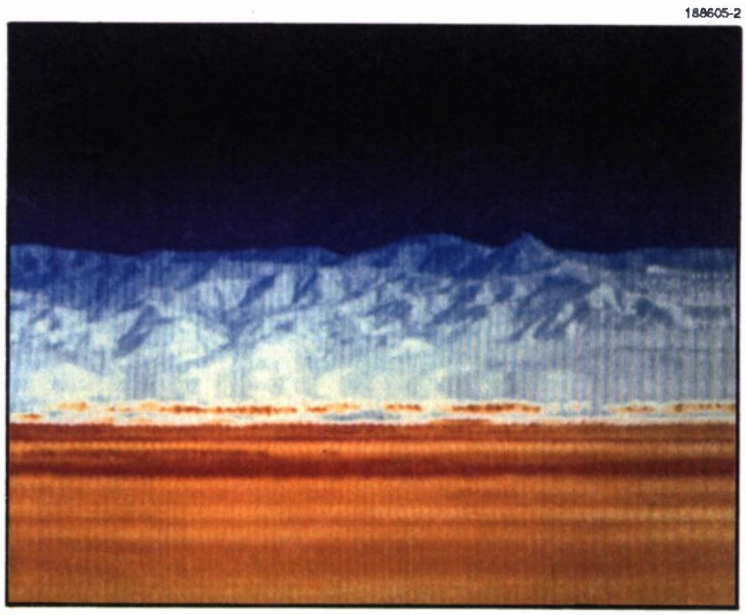

Figure 3. Single unprocessed frame of IRMS Dugway data.

detector (a Poisson random variable that may be approximated as normal). Assuming stationarity over time implies assuming that all frames in a sequence are spatially registered and that there is no moving clutter. Nonstationary spatial statistics correspond to the nonuniform intensity of the background scene.

An equivalent viewpoint is to consider the mean for a given pixel to be the image intensity in that pixel and the variance to correspond to the (photon plus thermal) noise level. The independence of samples then corresponds to each sample having an independent noise component, while the means correspond to the imaged scene.

The log-likelihood function $\mathcal{L}$ (which results from this data model) follows, where $r_{i,j,k}$ is the data sample in row i, column j, frame k, and N is the number of frames available (see Appendix A).

$$\mathcal{L} = \sum_{(i,j,k)\in S} d_{i,j,k} \tag{1}$$

$$d_{i,j,k} = \frac{(r_{i,j,k} - \hat{\mu}_{i,j})^2}{\hat{\sigma}^2_{i,j}} \tag{2}$$

$$\hat{\mu}_{i,j} = \frac{1}{N}\sum_{n=0}^{N-1} r_{i,j,n} \tag{3}$$

$$\hat{\sigma}^2_{i,j} = \frac{1}{N}\sum_{n=0}^{N-1} (r_{i,j,n} - \hat{\mu}_{i,j})^2 \tag{4}$$

The exact underlying means and variances are $\mu_{i,j}$ and $\sigma^2_{i,j}$ and are presumed unknown. Target detection is accomplished by comparing $\mathcal{L}$ to a threshold.

Set S is the set of space (i,j) and time (k) indices that corresponds to the target motion hypothesis. As an example, consider a target that moves with speed v pixels/s in the (i,j) plane at an angle θ. For a frame-to-frame period of T s, set S is

$$S = \{(i + vTk\cos(\theta),\ j + vTk\sin(\theta),\ k);\ k = 0,\ldots,N-1\} \quad , \tag{5}$$

where the noninteger coordinates are rounded to the nearest integer values.

1.2 Single Pixel Statistics

The term $d_{i,j,k}$ in the formula for the log-likelihood function is referred to as the "normalized" data. Selection of detection thresholds and the resulting probabilities of false alarm and detection depend on the statistics of $d_{i,j,k}$ and $\mathcal{L}$. The theoretical distribution $F_d(x|N)$ of $d_{i,j,k}$ has been derived and shown to be an instance of the beta distribution (see Appendix B).

$$F_d(x|N) = F_B\left(\frac{x}{N-1}\middle|\frac{1}{2}, \frac{N-2}{2}\right) \tag{6}$$

It is interesting to note that the statistics of $d_{i,j,k}$ depend only on the number of frames processed and not on the terms $\mu_{i,j}$ and $\sigma^2_{i,j}$ related to the specifics of the background clutter. Thus the effects of clutter are removed from determination of false alarm rates.

Clutter does have an effect on the single pixel statistics when targets are present. The pixel variance $\sigma^2_{i,j}$ is the noise component of the signal-to-noise ratio (SNR) and is related to the pixel mean $\mu_{i,j}$. (Specifically, if the data values were the number of photons received, then the mean and variance of a pixel would be equal.) It is shown in Appendix B that an instantaneous signal-to-noise ratio $\mathrm{SNR_i} = s^2/\sigma^2$ can be defined, where s is the target amplitude component of the unnormalized pixel data, and σ^2 is the noise power component. Then the conditional distribution for a single normalized pixel is the noncentral beta distribution

$$F_d(x|N, \mathrm{SNR_i}) = F_{B'}\left(\frac{x}{N-1}\middle|\frac{1}{2}, \frac{N-2}{2}, \frac{N-1}{N}\cdot \mathrm{SNR_i}\right) \quad . \tag{7}$$

Figure 4 shows the theoretical normalized pixel probability distribution for various values of $\mathrm{SNR_i}$ [expressed in decibels, $10\log(\mathrm{SNR_i})$].

A comparison of theory with empirically derived statistics can be used to validate the data model and the use of the resulting maximum likelihood detection algorithm. Figures 5 through 7 compare the theoretical distribution for a single normalized pixel and experimentally derived distributions for a variety of image sequences. These comparisons are done for the noise-only case (no target).

Figure 5 compares theory and experiment for 15 frames of visible band data obtained from the ETS sensor, which is a ground-based staring sensor, looking at a background of stars. Although the stellar background is spatially nonstationary, there is good agreement between the two curves.

Figure 6 compares theory and experiment for 10 frames of the Longjump LWIR data obtained from the IRMS scanning sensor, which is looking at a background of sky, mountains, and hills. Again, there is good agreement.

Figure 7 compares theory with 10 frames of LWIR data from Dugway, obtained from the IRMS sensor. Background clutter includes sky, mountains, and desert. Departure from theory is due in part to frame registration errors but may include other transient (time varying) interference as well. In general, data that are not temporally stationary will disagree with this theory.

1.3 False Alarm Statistics

Once the single pixel statistics are known, it is possible to determine the theoretical probability of false alarm and compare this theory to experimental data. The probability of false alarm is

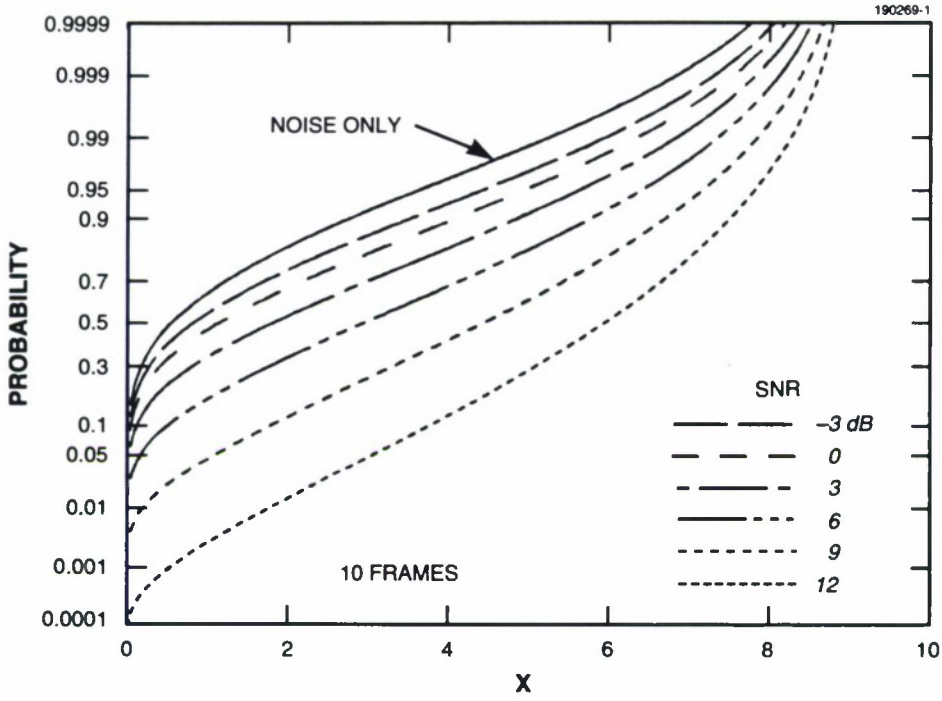

Figure 4. Theoretical normalized pixel probability distribution for different SNR_i.

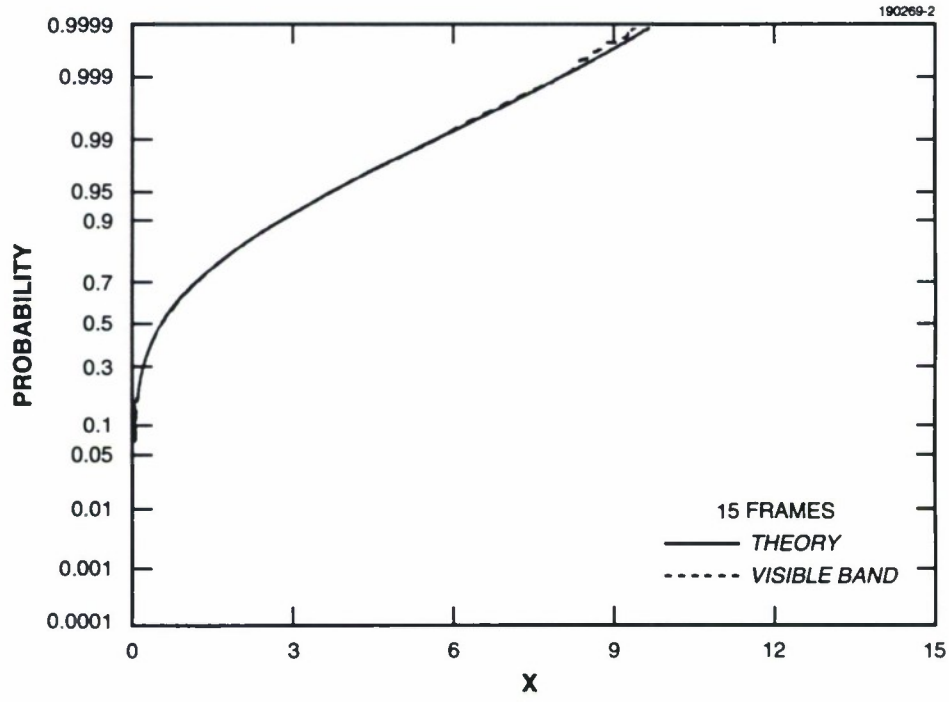

Figure 5. Single normalized pixel probability distribution of ETS Magellan data.

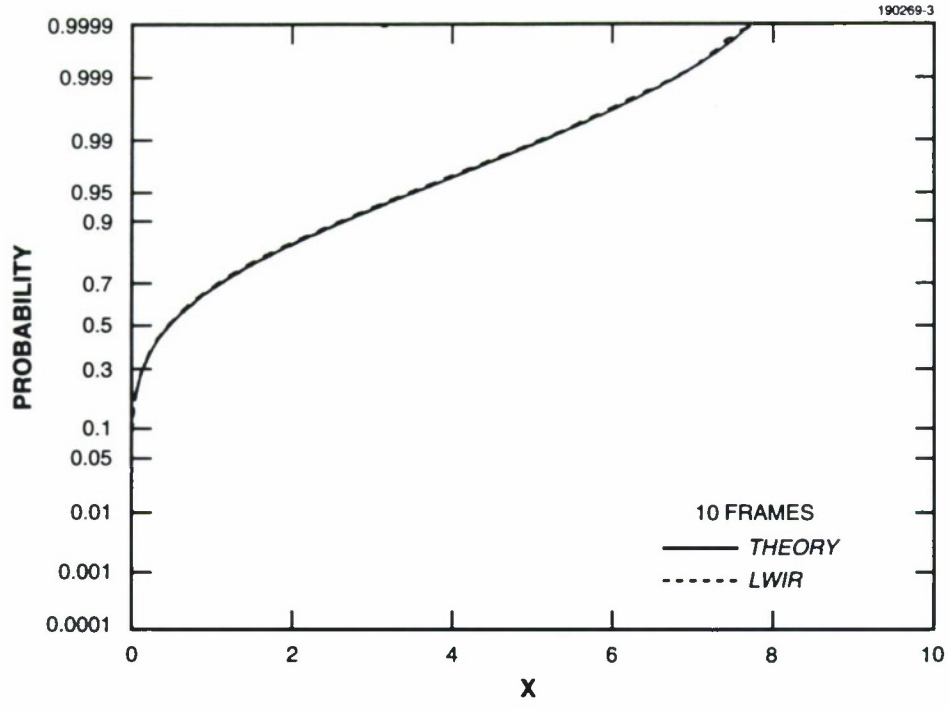

Figure 6. Single normalized pixel probability distribution of IRMS Longjump data.

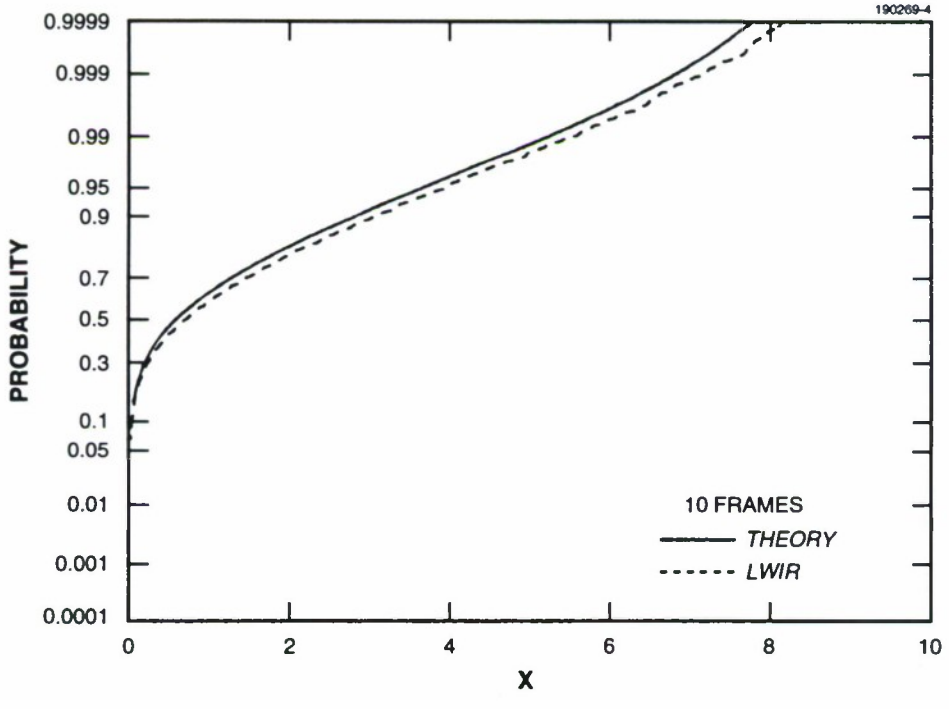

Figure 7. Single normalized pixel probability distribution of IRMS Dugway data.

defined as the probability that the log-likelihood function will exceed the detection threshold when no target is present. System false alarm rate is determined by combining the probability of false alarm with the number of pixels, the number of velocity hypotheses tested, and the data collection time.

Using the definitions

$$\begin{aligned} N_p &= \text{number of pixels in one frame} \\ N_v &= \text{number of velocity hypotheses} \\ N &= \text{number of image frames processed} \\ T &= \text{time to collect one image frame} \\ t &= \text{detection threshold} \\ R &= \text{false alarm rate,} \end{aligned}$$

the false alarm rate may be determined as the number of false alarms per second from the formula

$$R = \frac{N_p N_v \Pr\{\mathcal{L} \geq t|N\}}{NT} \quad . \tag{8}$$

The probability term $\Pr\{\mathcal{L} \geq t|N\}$ is computed as the N-fold convolution of single pixel density functions f_d with the complement of a unit step function $s(x)$.

$$\Pr\{\mathcal{L} \geq t|N\} = f_d * \cdots * f_d * (1 - s)(t) \tag{9}$$

This computation is implemented using numerical integration on the beta density functions (see Appendix C).

As an example of the false alarm rate, testing 1,000 velocity hypotheses on 10 frames of IRMS data results in

$$R = \frac{(400 \times 3480) \times 1000 \times 10^{-8}}{10 \times 1} \tag{10}$$

$$= 1.392 \text{ false alarms/s.} \tag{11}$$

The detection threshold t is assumed to be chosen so that the probability of a false alarm from a single target position and velocity test is 10^{-8}. The full frame of the IRMS data is used with a corresponding collection rate of 1 frame/s.

The validity of the false alarm rate calculation depends on the accuracy of the probability of false alarm term in the expression for R. For the probability of false alarm term to show agreement between theory and experiment at a level of 10^{-8}, the theoretical and experimental probability distributions (i.e., $\Pr\{\mathcal{L} < t|N\} = 1 - \Pr\{\mathcal{L} \geq t|N\}$) of the log-likelihood function should agree to eight significant digits.

Theoretical and experimental probabilities of false alarm are compared in Figures 8 through 10. Experimental probabilities are determined by testing 10^4 velocity hypotheses on 1.8×10^5 pixels of the visible band data and 1.4×10^5 pixels of IR data. Thus the total number of hypotheses tested for each experiment is approximately 10^9. For each data set, a histogram is formed from the values of the log-likelihood function for these trials. The probability curve is then easily computed from the histogram.

Figure 8 shows false alarm statistics for 15-frame processing of the ETS Magellan visible band data set, and Figure 9 shows 10-frame processing of IRMS Longjump LWIR data. These data sets show good agreement between theory and experiment (the two curves are difficult to distinguish!). Specifically, the two curves agree at probabilities down to at least 10^{-8}. Figure 10 shows 10-frame processing of IRMS Dugway LWIR data.

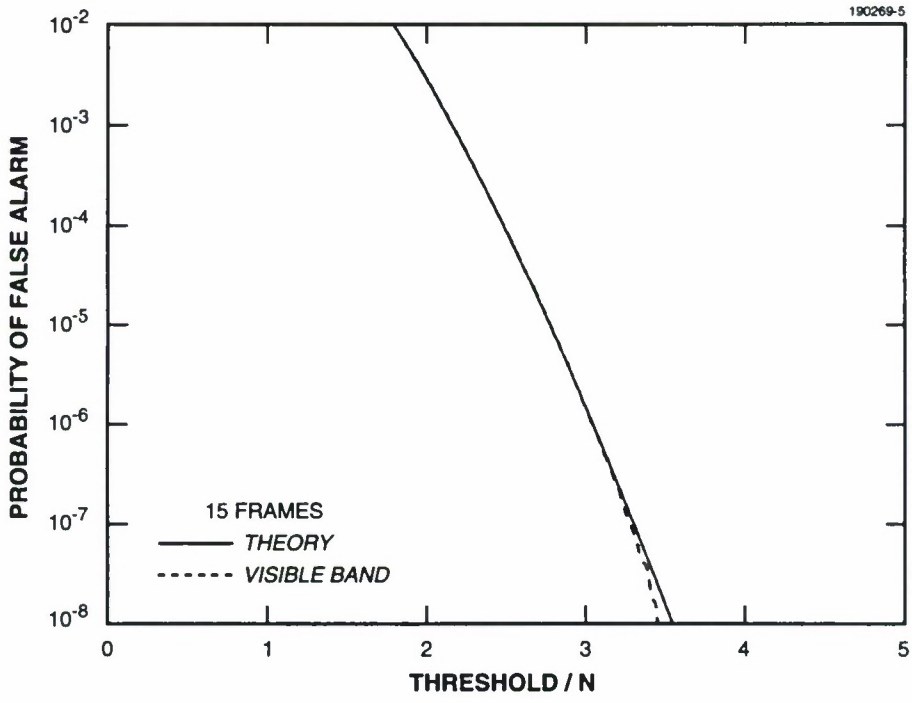

Figure 8. False alarm probability for ETS Magellan data.

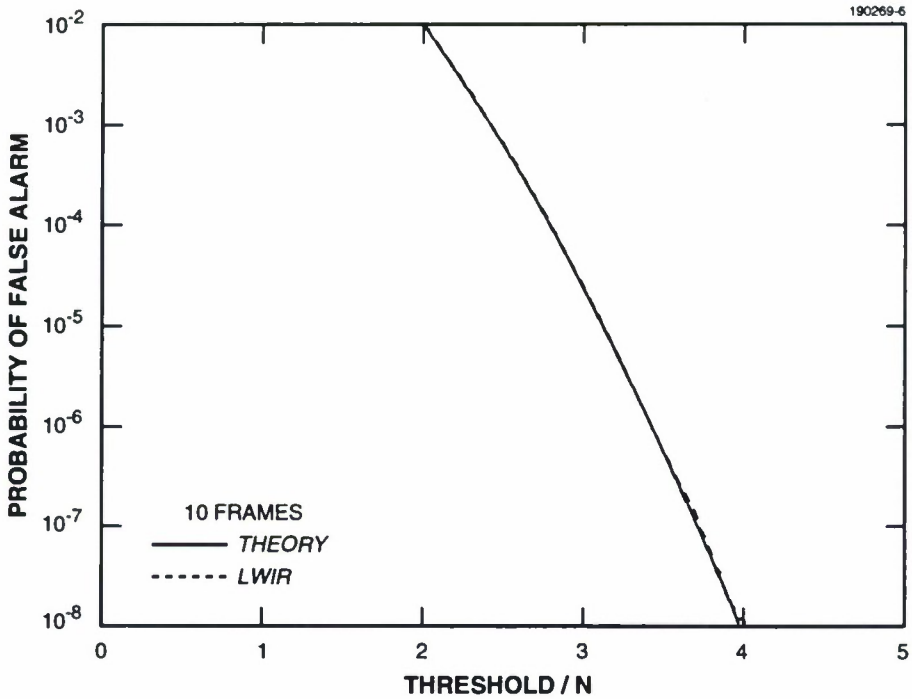

Figure 9. False alarm probability for IRMS Longjump data.

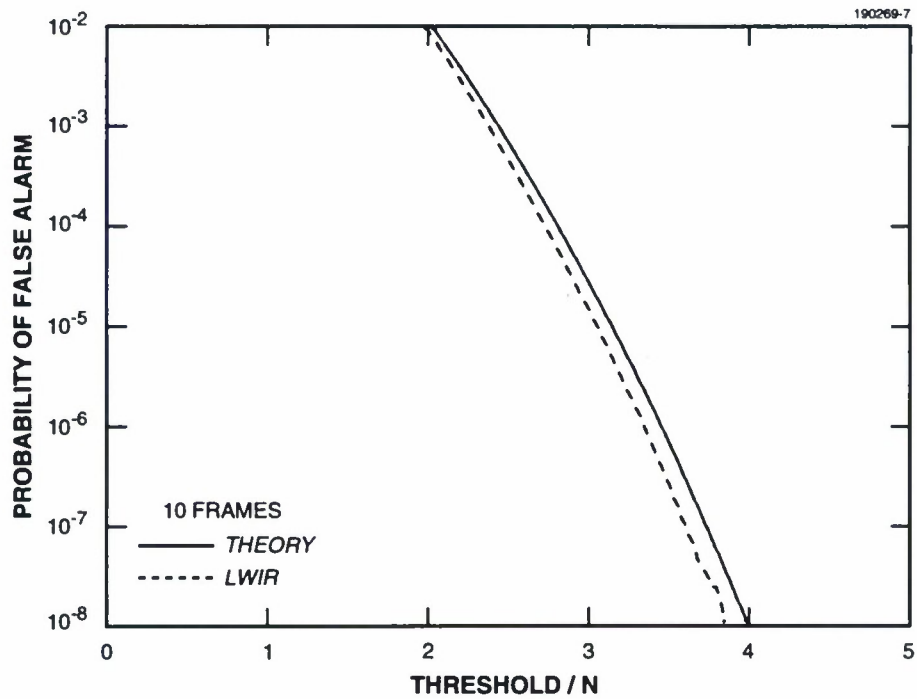

Figure 10. False alarm probability for IRMS Dugway data.

1.4 Detection Probability and Examples

As noted in Appendix C, the probability of detection depends on the SNR of the normalized pixels summed in the velocity hypothesis. The exact SNR distribution depends on the background clutter and is difficult to specify.

A simple case of the SNR distribution for uniform background clutter is discussed in Appendix C. Assuming that the dominant noise component is photon noise, the noise variance (power) of a pixel is proportional to the mean, which in turn corresponds to the pixel intensity. Thus the noise component of the SNR depends on the background clutter scene. The signal (target) component is also derived from a photon count and in the absence of other fluctuations gives a noncentral chi-square distribution. For uniform intensity background clutter the SNR distribution can be modeled as a constant times a chi-square random variable. For this simple case the detection probabilities depend on both the SNR and the target signal power. Other SNR models also depend on the clutter intensity distribution.

As an example, Figure 11 shows the theoretical probability of detection when the same number of target photons are received in each pixel, and σ^2 is identical across all pixels. In other words, $\mathrm{SNR_i}$ is assumed constant. In this case, $N = 10$ frames are assumed to be processed.

In the detection examples that follow, an effective signal-to-noise ratio, $\mathrm{SNR_{eff}}$, is estimated from the data. This value is defined as the value of $\mathrm{SNR_i}$, which has a normalized pixel mean (expected value) equal to the sample average of normalized pixels along the hypothesized target path. These two pixel quantities are not the same, because the expected value is determined for a single value of $\mathrm{SNR_i} = s^2/\sigma^2$, and the sample average is determined from data where both s^2 and σ^2 vary among pixels. Thus the term "effective SNR" is used. Figure 12 shows the normalized pixel mean as a function of $\mathrm{SNR_i}$ for 10- and 15-frame processing.

Figure 13 shows a detection example for the ETS Magellan visible band data set. Approximately 600 velocity hypotheses are applied to these data (418×420 pixels/frame). The false alarm rate for a single hypothesis test is set to 10^{-8}, and the expected number of false alarms is 0.9. (The target motion hypothesis is required to fit entirely within the data in this experiment, so that not all combinations of position and velocity are used.) The estimated values of $\mathrm{SNR_{eff}}$ for these targets are 10.3 and 15.3 dB.

Figure 14 shows a detection example for the IRMS Longjump LWIR data set. Approximately 1,000 velocity hypotheses are applied to a 400×400 subimage of the data. The false alarm rate for a single hypothesis test is set to 10^{-8}, and the expected number of false alarms is 1.4. (As above, not all combinations of position and velocity are used.) The estimated value of $\mathrm{SNR_{eff}}$ for this target is 17.3 dB.

Figure 15 shows a detection example for the IRMS Dugway LWIR data set. Approximately 1,800 velocity hypotheses are applied to a 400×500 subimage of the data. The false alarm rate for a single hypothesis test is set to 10^{-8}, and the expected number of false alarms is 1.4. (Again, not

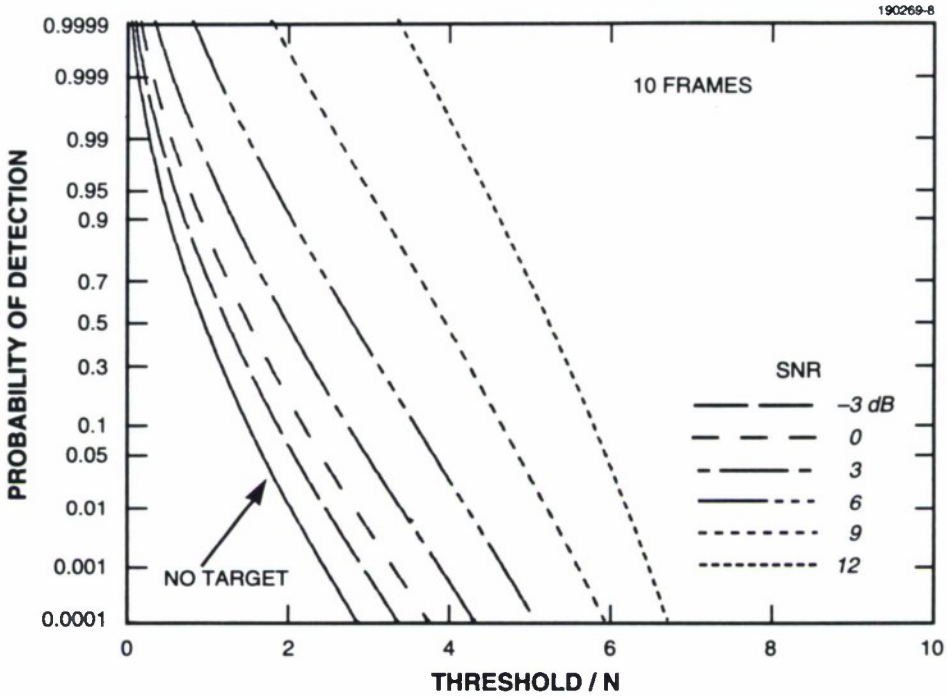

Figure 11. Theoretical probability of detection for constant SNR_i.

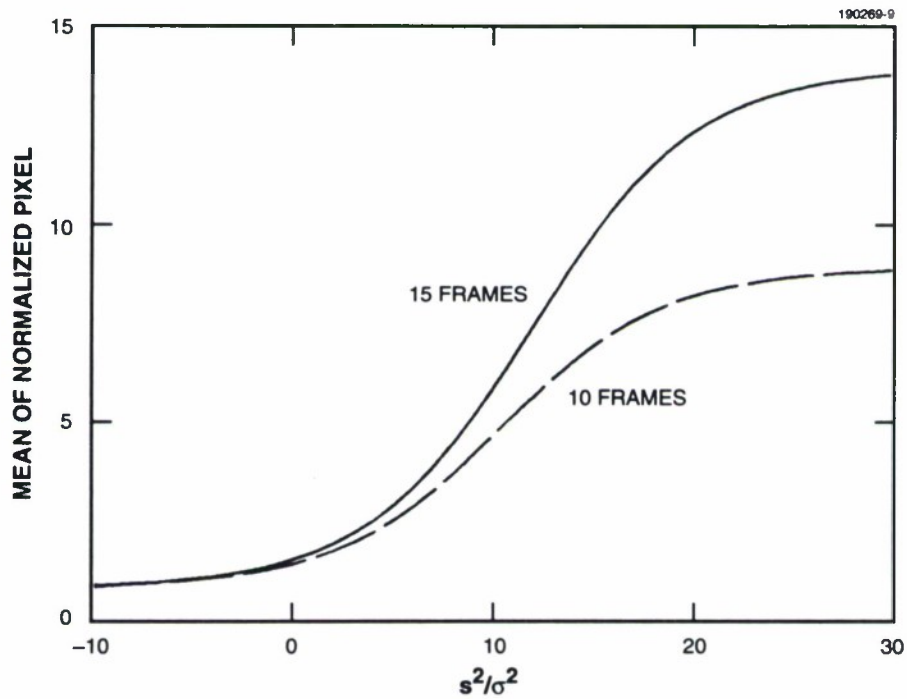

Figure 12. Expected value (mean) of normalized pixels as a function of SNR_i.

all combinations of position and velocity are used.) The upper detection is a target, and the lower detection is a false alarm. The estimated value of SNR_{eff} for the actual target is 9.5 dB.

Target-related false alarms can occur when a hypothesized target path intersects the actual path of a strong target. From Equation (1) it is clear that a single, strong, normalized pixel can cause the log-likelihood function $\mathcal{L}$ to exceed a detection threshold. One way to reduce the false alarms related to strong targets and clutter discretes is to impose a model of the target statistics in the likelihood function derivation. This approach has the disadvantage of depending on the target and clutter models, as well as resulting in a much more complex formula for the log-likelihood function. A different approach is to require that any detection also has at least a certain number of strong pixels. This concept is the basis for the binary detection algorithm discussed in Section 2.

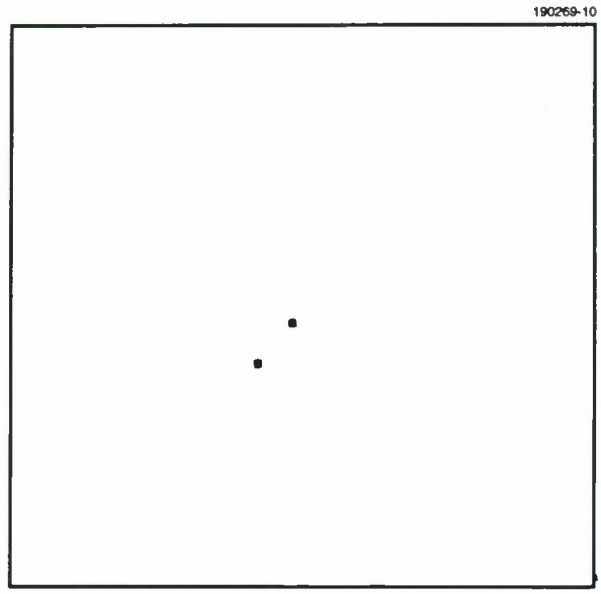

(a)

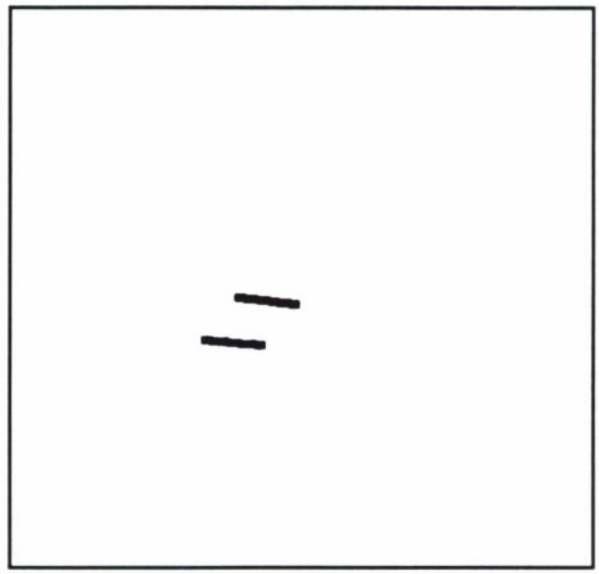

(b)

Figure 13. Target detection for ETS Magellan data. (a) Detected target locations. (b) Extrapolated target motion.

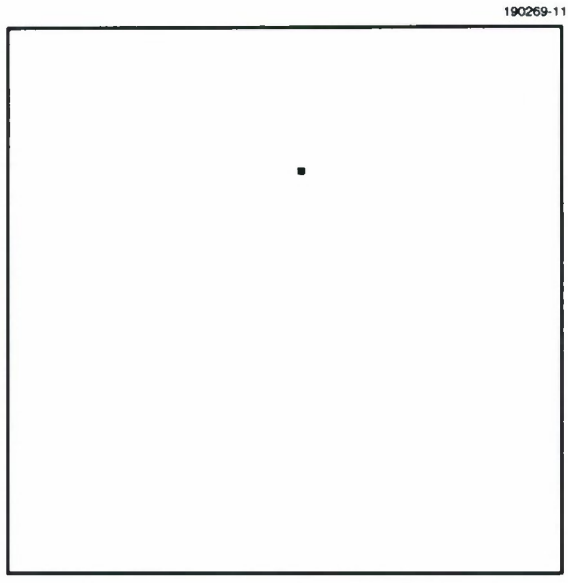

(a)

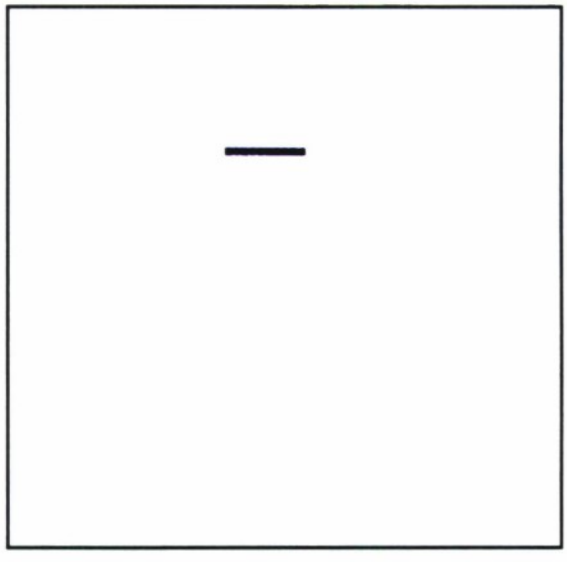

(b)

Figure 14. Target detection for IRMS Longjump data. (a) Detected target locations. (b) Extrapolated target motion.

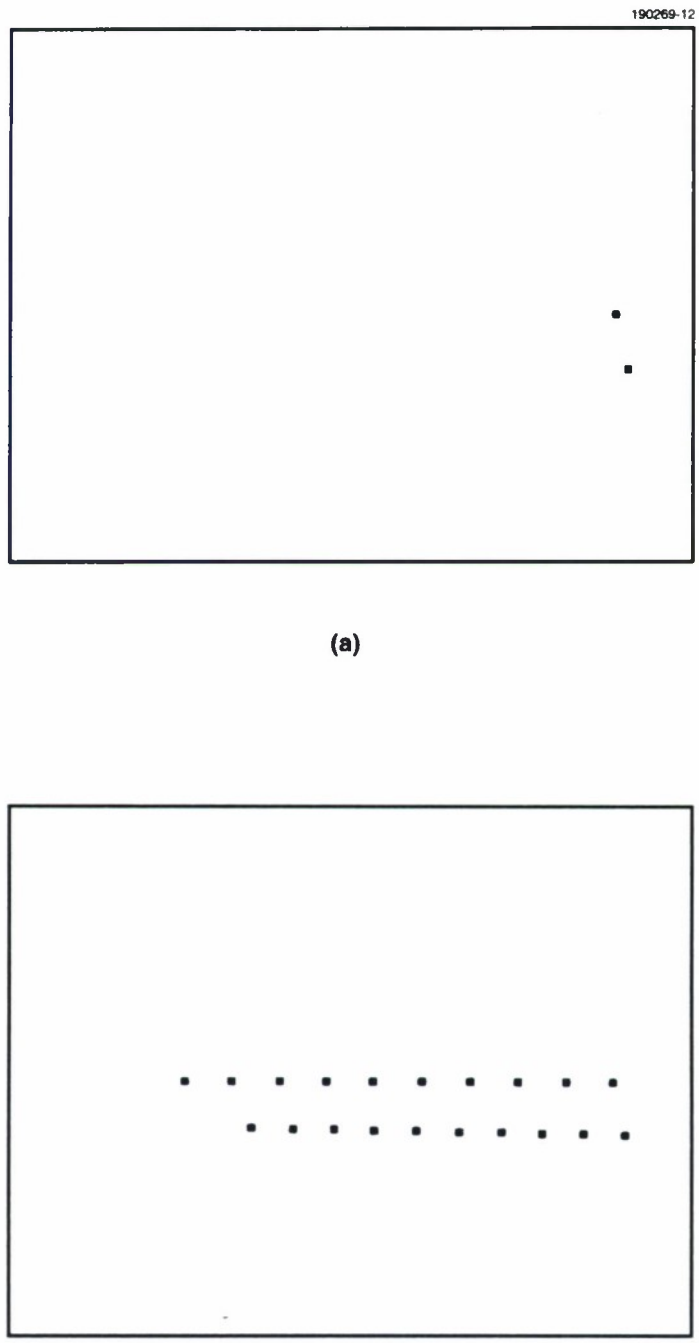

Figure 15. Target detection for IRMS Dugway data. (a) Detected target locations. (b) Extrapolated target motion.

2. BINARY INTEGRATION ALGORITHM AND ARCHITECTURE

For many applications, the algorithm discussed in Section 1 is computationally intensive. This section describes an algorithm for a binary integration approach to velocity filtering. Binary integration is of interest as a means of reducing both memory and computation rate requirements at a small loss (typically less than 2 dB) in processing gain. Also presented is an implementation architecture that is suitable for a small applications specific integrated circuit (ASIC), which could be attached to a general purpose signal processor.

An overview and performance measures of binary integration are given in Section 2.1. The algorithm is described mathematically in Section 2.2. An architecture for efficient implementation is described in Section 2.3. Extension of this algorithm to nonscanned sensors, where targets form streaks within an image frame, is discussed in Section 2.4.

2.1 Algorithm and Performance

Binary integration, a technique that is well known in the radar community, is often referred to as an "M-out-of-N detector" [1, 2]. A variation of binary integration is also used in the Maximum Value Projection algorithm implemented on the Space-Based Visible processor [3].

The relationship between binary integration and other electro-optic signal processing functions is shown in Figure 16. Typically, sensor data may be corrected (e.g., for gamma circumvention in space applications) and, in the case of scanning sensors, time-delay integrated to improve target SNR. Most moving target detection algorithms also require some form of frame registration. The remainder, data normalization/quantization and velocity filtering, form the moving target detection algorithm. Binary integration addresses these last two parts.

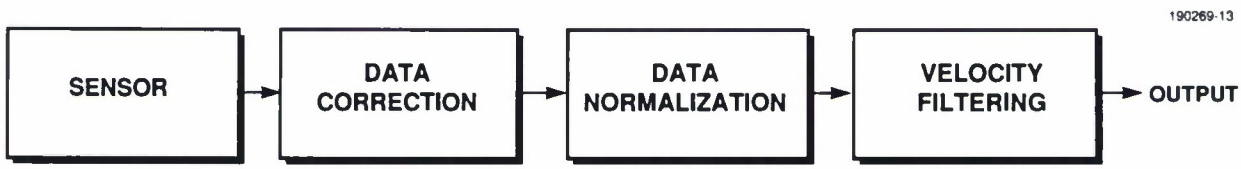

Figure 16. Signal processing functions.

The binary integration approach may be divided into four steps:

1. Data normalization
2. Binary quantization

3. Integration (summation) over the velocity hypotheses

4. Threshold detection of the integration results.

Data may be normalized using a variety of techniques. The maximum likelihood algorithm in Section 1 suggests that normalized data $d_{i,j,k}$ be obtained from unprocessed data $r_{i,j,k}$ according to

$$d_{i,j,k} = \frac{(r_{i,j,k} - \hat{\mu}_{i,j})^2}{\hat{\sigma}^2_{i,j}} \tag{12}$$

$$\hat{\mu}_{i,j} = \frac{1}{N}\sum_{k=0}^{N-1} r_{i,j,k} \tag{13}$$

$$\hat{\sigma}^2_{i,j} = \frac{1}{N}\sum_{k=0}^{N-1}(r_{i,j,k} - \hat{\mu}_{i,j})^2 \quad , \tag{14}$$

where i,j are the pixel indices and k is the image frame index. Binary quantized data $b_{i,j,k}$ are then obtained by comparing $d_{i,j,k}$ with a fixed threshold t.

$$b_{i,j,k} = \begin{cases} 0, & d_{i,j,k} < t \\ 1, & d_{i,j,k} \geq t \end{cases} \tag{15}$$

The integration step is also called velocity filtering. Samples in (i,j,k) are integrated along a hypothesized target velocity vector. This velocity hypothesis corresponds to the velocity filter.

The number of samples used in integration depends on sensor type. For a scanning sensor, a target moves less than one pixel during the time the target is scanned; however, the total scanning time of a frame is typically large enough so that a target moves several pixels from one frame to the next. Thus a target streak in (i,j,k) appears as a dotted instead of solid line. In this case, the integration step requires summing only 1 pixel/frame for spatially unresolved targets.

Let $s_{i,j}$ be the result of summing (integrating) over the data for a target that has initial position i,j and frame-to-frame velocity components u,v in the x,y directions. The result $s_{i,j}$ is compared with a threshold in order to achieve a detection. (This summation and comparison is the M-out-of-N detector.) The quantity $s_{i,j}$ is computed according to the formula[1]

[1]In general, velocity components u,v are floating point numbers; indices $i+uk$ and $j+vk$ are then taken to be the nearest integer values. This method is called nearest neighbor interpolation.

$$s_{i,j} = \sum_{k=0}^{N-1} b_{i+uk,j+vk,k} \quad . \tag{16}$$

The performance of the binary integration algorithm can be given in terms of the probabilities of detection and false alarm by computing the probability that $s_{i,j}$ meets or exceeds the threshold M for a given SNR. Let p be the probability that a single normalized pixel exceeds threshold t,

$$p = 1 - F_d(x|N, \mathrm{SNR_i}) \tag{17}$$

$$= 1 - F_{B'}\left(\frac{x}{N-1}\middle|\frac{1}{2}, \frac{N-2}{2}, \frac{N-1}{N} \cdot \mathrm{SNR_i}\right) \quad . \tag{18}$$

Using the constant $\mathrm{SNR_i}$ example discussed in Section 1, the probability of detection P_D is obtained as the probability of a binomial random variable with parameter p having at least M occurrences out of N trials.

$$P_D = \Pr\{s_{i,j} \geq M\} \tag{19}$$

$$= \sum_{m=M}^{N} \binom{N}{m} p^m (1-p)^{N-m} \tag{20}$$

The corresponding probability of false alarm P_{FA} is obtained by setting $\mathrm{SNR_i} = 0$.

The two thresholds, t and M, are usually chosen to maximize the P_D for a particular operating point in terms of $\mathrm{SNR_i}$ and P_{FA}. This maximization can be performed by computing, for each possible value of $M = 0, \ldots, N$, the value of t that gives the desired P_{FA}. The (t, M) pair to be used is that which maximizes the value of P_D for the required $\mathrm{SNR_i}$.

As an example, consider $N = 10$ frames and let the operating point for this optimization be $P_{FA} = 10^{-8}$ and $\mathrm{SNR_i} = 10$. The maximization of P_D yields $M = 7$ and $t = 3.310$. Probabilities of detection and false alarm can be plotted for a constant M or t.

Figure 17 shows the probability of detection as a function of t, the single pixel threshold, for $M = 7$ and several different $\mathrm{SNR_i}$. Figure 18 shows the false alarm probability.

Figure 19 shows the probability of detection as a function of M, for $t = 3.310$ and several different $\mathrm{SNR_i}$. Figure 20 shows the false alarm probability.

A comparison of Figure 17 with Figure 11 indicates the loss in SNR for the binary integration algorithm. For the specified $P_{FA} = 10^{-8}$, the binary algorithm requires less than 11-dB $\mathrm{SNR_i}$ target to achieve the same detection probability as the full precision maximum likelihood algorithm with a 10-dB $\mathrm{SNR_i}$ target, indicating a loss less than 1-dB. This loss is similar to that obtained when binary integration is used in radar processing [1, 2].

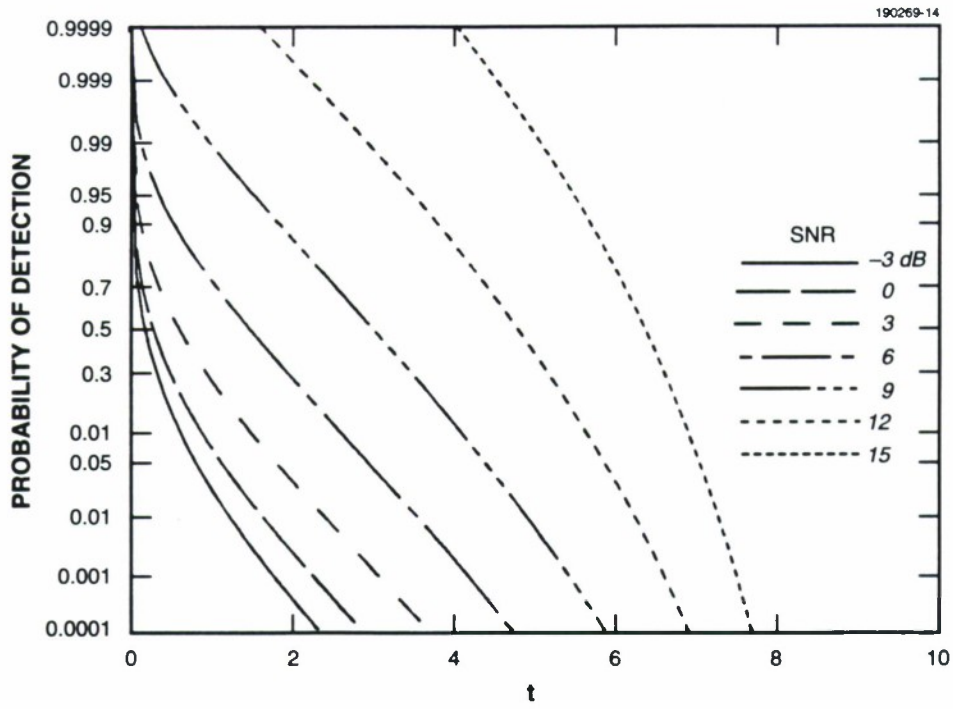

Figure 17. Probability of detection for binary integrator, $N = 10$ frames, $M = 7$.

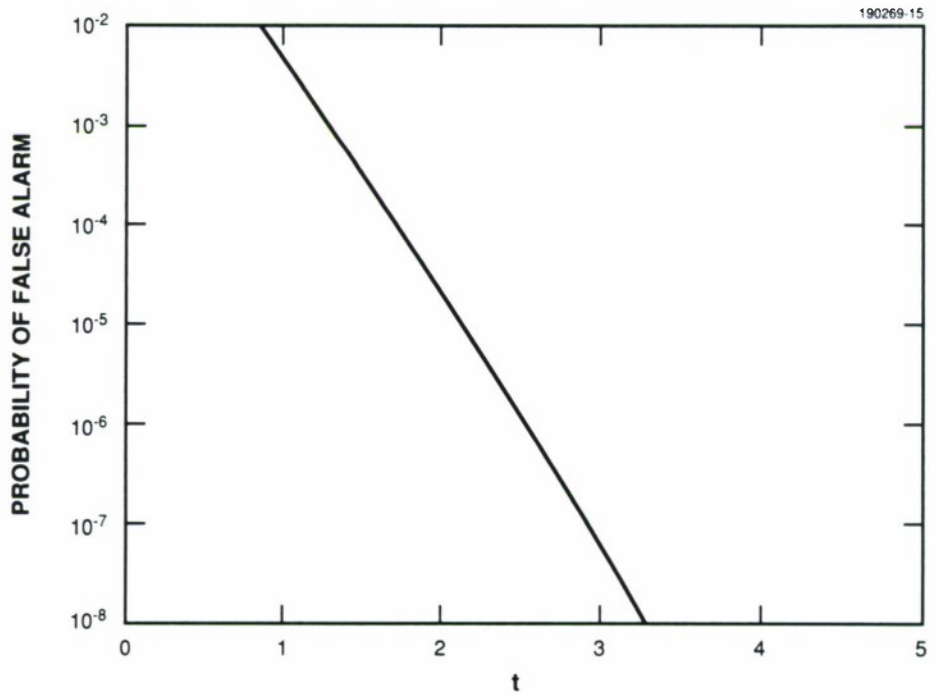

Figure 18. Probability of false alarm for binary integrator, $N = 10$ frames, $M = 7$.

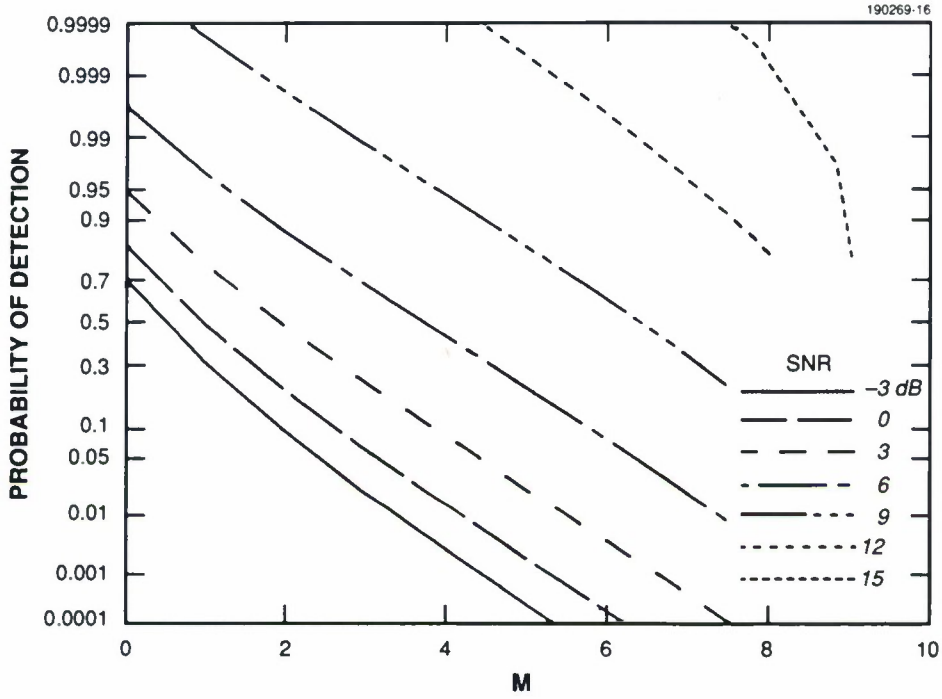

Figure 19. Probability of detection for binary integrator, $N = 10$ frames, $t = 3.310$.

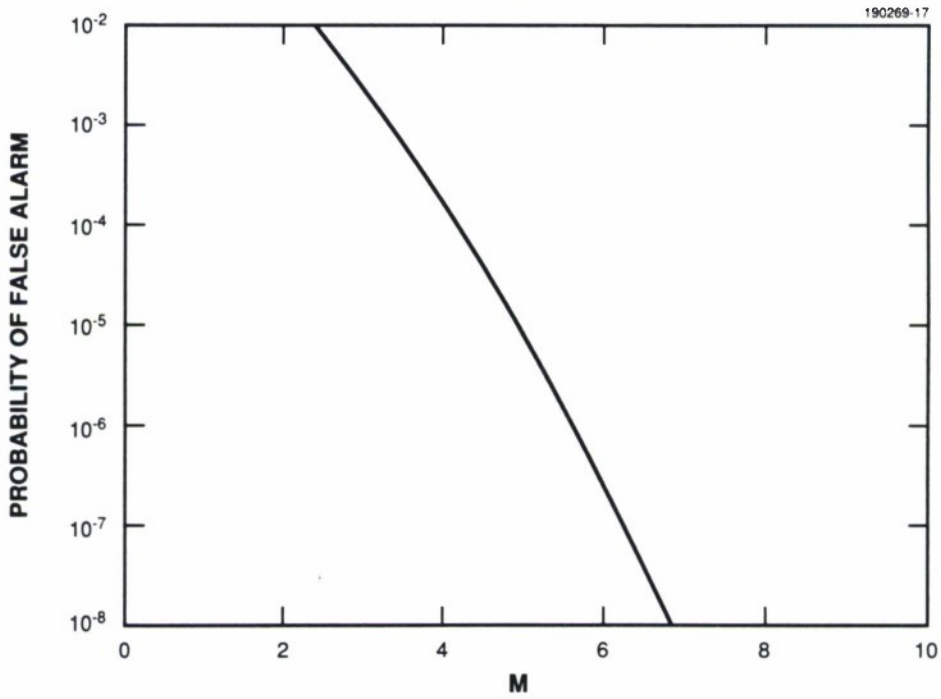

Figure 20. Probability of false alarm for binary integrator, $N = 10$ frames, $t = 3.310$.

2.2 Efficient Integration Algorithm

Computationally, the most intensive step is integration. Efficiency is attained by reducing the number of data accesses required in testing a given velocity hypothesis on many possible target positions.

Let M_x, M_y be the frame size in the x, y dimensions, respectively. There are $\sim M_x M_y$ possible initial target positions. For each velocity hypothesis, integration and detection of N data frames can be accomplished straightforwardly by summing N samples (one from each frame) for each possible target position. This method requires $M_x M_y N$ additions or comparisons and $M_x M_y N$ data accesses. The objective of the algorithm presented here is to reduce the number of data accesses to $M_x M_y$ and to perform N additions with each. Thus it will be shown that the $M_x M_y$ possible initial target positions can be tested at an average cost of only one data access per test. The algorithm derivation that follows is rather mathematical and may be skipped in favor of reading the step-by-step description given at the end of this section.

The first step is to pack N frames of binary data into N-bit integers, $a_{i,j}$,

$$a_{i,j} = \sum_{k=0}^{N-1} b_{i,j,k} 2^k \quad , \tag{21}$$

where

$$0 \leq i < M_x \tag{22}$$

$$0 \leq j < M_y \quad . \tag{23}$$

The above formula for $s_{i,j}$ can be written as

$$s_{i,j} = \sum_{k=0}^{N-1} B_k(a_{i+uk,j+vk}) \quad , \tag{24}$$

where $B_k(z)$ is bit k of z.

Now consider the computation of $s_{i+u,j+v}$.

$$s_{i+u,j+v} = \sum_{k=0}^{N-1} B_k(a_{i+u+uk,j+v+vk}) \tag{25}$$

$$= \sum_{k=1}^{N} B_{k-1}(a_{i+uk,j+vk}) \tag{26}$$

It is important to note that $N-1$ of the data accesses required (that is, indices of $a_{i,j}$) are identical between $s_{i,j}$ and $s_{i+u,j+v}$. If the two summations can be performed simultaneously (which is possible, using the architecture described in Section 2.3), then accessing a single additional composite data sample permits an additional integrator output to be computed. This idea can be carried forward so that each additional data access permits an additional integrator output to be computed.

This savings can be generalized. For simplicity, assume that $u \geq 0$ and $v \geq 0$. (The algorithm can be applied to negative velocities as well.) Note that

$$s_{i+nu,j+nv} = \sum_{k=n}^{N+n-1} B_{k-n}(a_{i+uk,j+vk}) \quad . \tag{27}$$

For each i,j pair a set of integrator outputs can be computed for some range of n. One needs to consider the set of i,j indices and the range of n. The set of i,j is easily determined. Assuming that all possible values of n are to be used, it is only necessary to search set S,

$$S = \{(i,j);\ 0 \leq i < u \text{ or } 0 \leq j < v\} \quad . \tag{28}$$

This set is illustrated by the dotted region in Figure 21. Initial target positions outside this set are obtained for values of $n \neq 0$.[2] For example, the black circle within the dotted region indicates a particular i,j pair with $n = 0$. Values of $n > 0$ correspond to initial target positions indicated by the sequence of black circles in the clear region.

The range of n can now be computed. If the desire is to detect only those targets that do not enter or exit the field of view during the N frames, then the maximum value of n is determined by restricting n so that the indices $i+uk, j+vk$ in Equation (27) satisfy

$$\begin{aligned} 0 \leq\ & i+uk\ < M_x - 0.5 \\ 0 \leq\ & j+vk\ < M_y - 0.5 \end{aligned} \quad . \tag{29}$$

In this case

---

[2]This statement is not completely accurate; because u and v are floating point numbers and nearest neighbor interpolation is used, it is possible to miss some initial positions. These omissions can be eliminated by using the set $S = \{(i,j);\ 0 \leq i \leq u \text{ or } 0 \leq j \leq v\}$ at the expense of duplicating some initial positions. This additional expense is small relative to the overall cost.

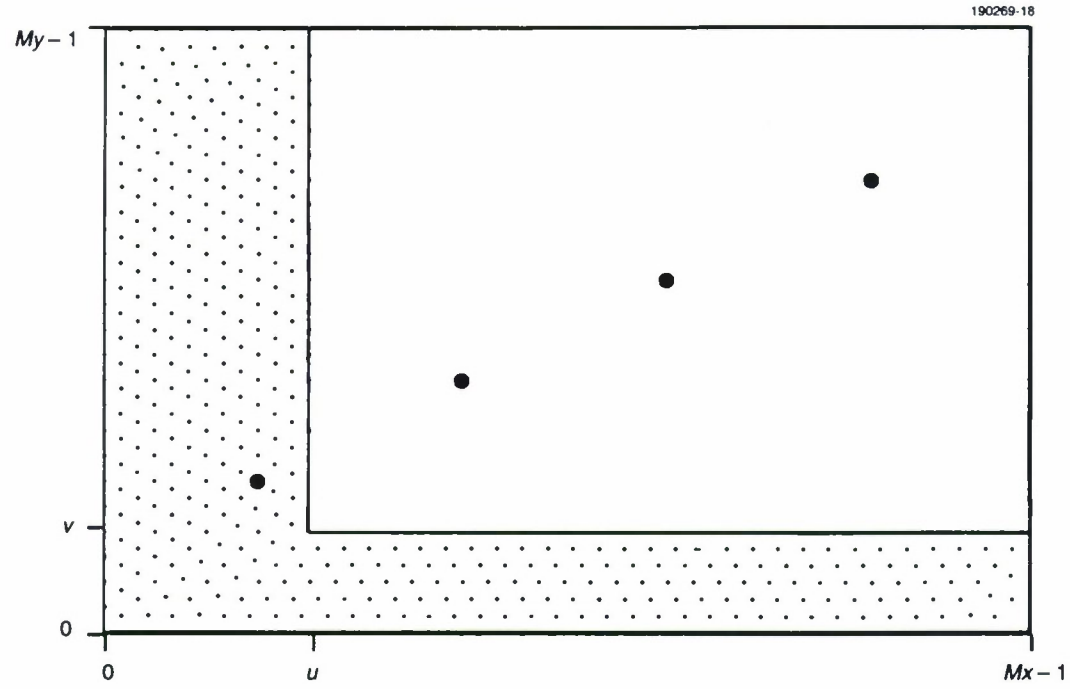

Figure 21. Search region for i, j.

$$0 \leq n < \min\left(\frac{M_x - 0.5 - i}{u}, \frac{M_y - 0.5 - j}{v}\right) - (N-1) \tag{30}$$

for $u \neq 0$ and $v \neq 0$. [If either $u = 0$ or $v = 0$, then the appropriate fraction is deleted from Equation (30).] The number of integrator outputs computed for a given i, j pair is then[3]

$$\left\lceil \min\left(\frac{M_x - 0.5 - i}{u}, \frac{M_y - 0.5 - j}{v}\right) \right\rceil - (N-1) \quad . \tag{31}$$

The number of data accesses [i.e., values of k determined from the bounds in Equation (29)] is

$$\left\lceil \min\left(\frac{M_x - 0.5 - i}{u}, \frac{M_y - 0.5 - j}{v}\right) \right\rceil \quad , \tag{32}$$

[3]The notation $\lceil x \rceil$ is used to indicate the *ceiling* of x, the smallest integer that is greater than or equal to x. Similarly, $\lfloor x \rfloor$ is the *floor* of x, the largest integer that is less than or equal to x.

and the ratio of outputs computed per data access is

$$1 - \frac{N-1}{\lceil \min((M_x - 0.5 - i)/u, (M_y - 0.5 - j)/v) \rceil} \quad . \tag{33}$$

This ratio approaches unity as the frame size becomes much larger than the distance a target moves from one frame to the next.

Alternatively, the range of n may be chosen to include those targets that enter or exit the field of view during the N frames. Admittedly, such targets must have a higher SNR to be detected. In this case the range of n is determined by the bounds

$$0 \leq i + u(N + n - 1) \tag{34}$$

$$0 \leq j + v(N + n - 1) \tag{35}$$

$$i + un < M_x - 0.5 \tag{36}$$

$$j + vn < M_y - 0.5 \quad , \tag{37}$$

which give the following range on n.

$$\max\left(1 - N - \frac{i}{u}, 1 - N - \frac{j}{v}\right) \leq n < \min\left(\frac{M_x - 0.5 - i}{u}, \frac{M_y - 0.5 - j}{v}\right) \tag{38}$$

Given the bounds on i, j and noting that n is an integer, the lower bound on n can easily be shown to be $1 - N$ so that the range of n becomes

$$1 - N \leq n < \min\left(\frac{M_x - 0.5 - i}{u}, \frac{M_y - 0.5 - j}{v}\right) \quad . \tag{39}$$

The number of integrator outputs computed for a given i, j pair is the number of values of n in the above equation,

$$\left\lceil \min\left(\frac{M_x - 0.5 - i}{u}, \frac{M_y - 0.5 - j}{v}\right) \right\rceil + N - 1 \quad . \tag{40}$$

The number of data accesses is identical to the previous case. The ratio of outputs per data access in this case is then

$$1 + \frac{N-1}{\lceil \min((M_x - 0.5 - i)/u, (M_y - 0.5 - j)/v) \rceil} \quad , \tag{41}$$

which is clearly greater than unity.

The resulting algorithm, which tests a given velocity hypothesis, is described in this series.

1. Let N be the number of image frames, each with size M_x, M_y in the x, y dimensions.
2. Let M be the detection threshold (i.e., the number of binary quantized frames in which a target must appear in order to have a detection).
3. Let $a_{i,j}$ be the composite of the binary data for pixel i, j and all frames, as described in Equation (21).
4. Let u, v be the frame-to-frame target movement in x, y for the desired velocity hypothesis, $u \geq 0$ and $v \geq 0$.
5. For each pair i, j such that $0 \leq i \leq u$ or $0 \leq j \leq v$, do the following:
   (a) Set $z_k = 0$ for $k = 1, \ldots, N-1$.
   (b) Let $L = \lceil \min((M_x - 0.5 - i)/u,\ (M_y - 0.5 - j)/v) \rceil - 1$.
   (c) For $n = 0, \ldots, L$, do the following:
      i. $s_{i+(n-N+1)u, j+(n-N+1)v} = z_{N-1} + B_{N-1}(a_{i+nu, j+nv})$. Compare this result with threshold M.
      ii. For $m = N-1, \ldots, 2$ set $z_m = z_{m-1} + B_{m-1}(a_{i+nu, j+nv})$.
      iii. Set $z_1 = B_0(a_{i+nu, j+nv})$.
   (d) For $n = L+1, \ldots, L+N-1$, the outcome is $s_{i+(n-N+1)u, j+(n-N+1)v} = z_{N+L-n}$. Compare this result with threshold M.

2.3 Architecture for Binary Integration

An architecture that implements the binary integration algorithm is shown in Figure 22. For a given i, j pair, this algorithm computes the $s_{i+nu, j+nv}$. The top row of adders and registers is used to implement the sums and partial sums $z_1, \ldots, z_{N-1}$. The subtracter compares the result z_{N-1} with the threshold M. Threshold crossings are stored in a FIFO with an index (counter output).

The bottom portion of Figure 22 generates the necessary addresses. The register stores a base address corresponding to the particular i, j pair in use. The counter generates the sequence $n = 0, \ldots$ to be used as an address to an offsets table, which is loaded from an external processor and contains the memory offsets corresponding to the pixel offset nu, nv. The table only needs to be changed when the velocity vector is changed. Finally, the adder combines the base address with the necessary offset, producing the memory address.

Operation of this architecture is straightforward. Initially, the top row of registers and the FIFO are set to zero. With each computation cycle the counter drives the address generation portion to access a particular word of memory. The composite binary sample at this address is

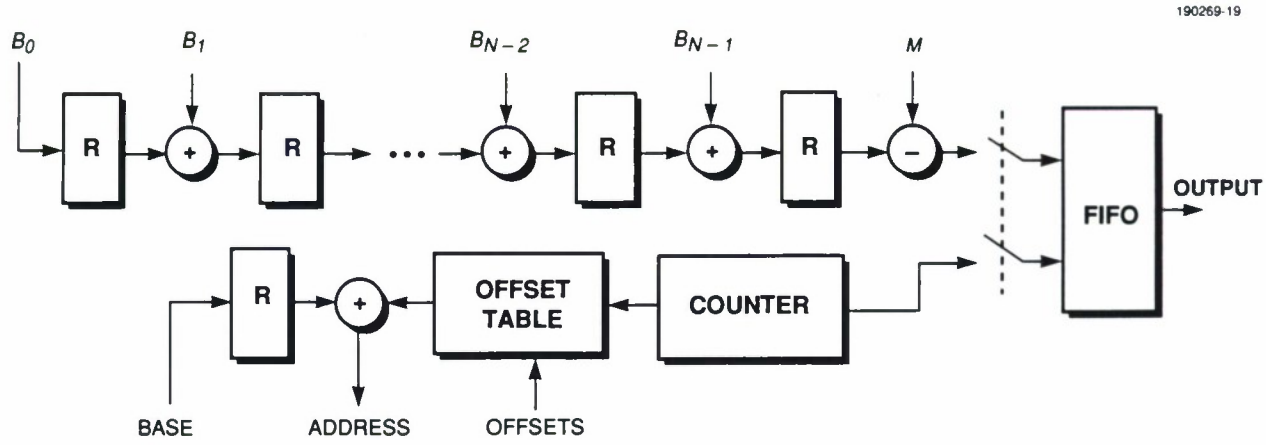

Figure 22. Architecture for integration step of algorithm.

presented to the inputs $B_0, \ldots, B_{N-1}$. These bits are added to the partial sums that are available from the register outputs. The output of the right-most register contains the completed sum, which is compared with the threshold M. At the end of each computation cycle, the adder outputs are stored in the registers, detections are stored in the FIFO, and the counter is incremented. Step 5(d) of the algorithm is implemented by reading $N-1$ words of zeros from memory. These zeros can be accessed by storing appropriate values in the offset table.[4] Note that the final register contents are all zeros so that the adder pipeline is initialized for the next i, j pair.

For typical parameter values, this architecture can be implemented in a small ASIC. For example, suppose $N \leq 16$, $M_x M_y \leq 10^6$, and $\max(M_x, M_y) \leq 4{,}000$. In this case the typical requirements are listed in Table 1. A 24-bit address bus is assumed for the memory. The FIFO depth is arbitrarily set to 256 words, although 64 might be sufficient. The left-most registers and adders require fewer bits than the right-most. It is clear that the circuit requirements are small.

Note that the architecture in Figure 22 is easily modified to permit the cascading of several such ASICs for large numbers of frames. In this case the input to the left-most register is now the output of an adder that has B_0 and an off-chip datum as inputs. In addition, the output of the right-most register is sent off-chip. Thus the top portion of additional ASICs may be cascaded with the final ASIC, which also performs detection and address generation. With this extension scheme, the limit on the total number of frames is set by the width of the registers, adders, and FIFO.

The velocity filter architecture is shown fitted into a signal processor architecture in Figure 23. There is a dual port memory for storing the data prior to registration, normalization, and

[4]High speed operation may require using pipeline registers at the address output and the B_k inputs.

TABLE 1

Architecture Component Requirements

Item	Amount
Register	78 bits
Adder (1 bit + k bit)	49 bits
Adder/Subtracter	29 bits
Counter	12 bits
RAM (offset table)	4K words × 20 bits
FIFO	256 words × 18 bits

quantization. A smaller memory (a single frame's worth) is used to separately store the binary quantized data. The CPU and a separate memory share a second bus, which allows the CPU to perform other computations while the velocity filter is in operation.

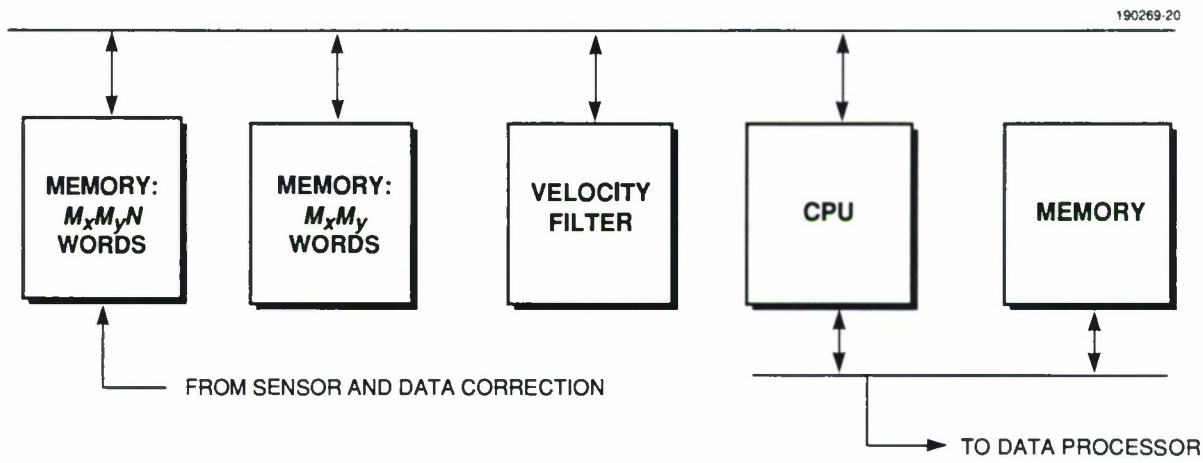

Figure 23. Architecture for binary integration.

To achieve sufficient processing performance, it may be necessary to have several velocity filters operating in parallel. One method for four filters (suggested by A. H. Huntoon) is shown in Figure 24. The composite memory is divided into a number of submemories equal to the number of velocity filters. Each submemory is assigned a contiguous set of columns of image data. The

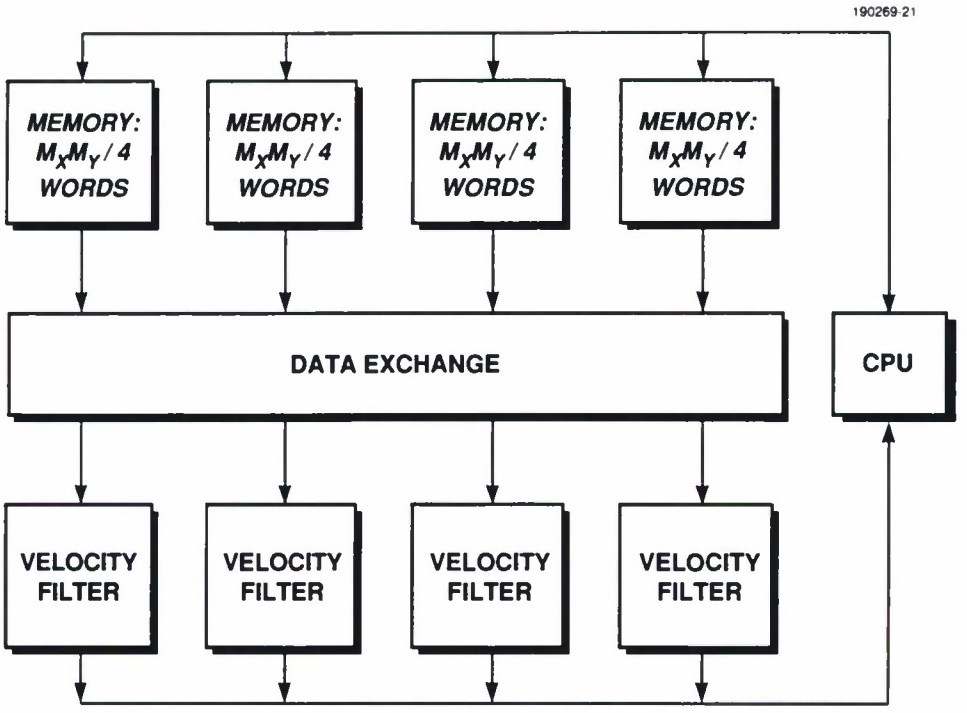

Figure 24. Parallel architecture for binary integration.

memories are connected to the velocity filters through a data exchange circuit. The sequence of tested target positions can be arranged so that during each memory access cycle, each velocity filter needs data from a separate submemory. In this case the (i, j) search region will be different from that depicted in Figure 21.

2.4 Extending the Algorithm to Nonscanning Sensors

With a scanned sensor, a moving target is expected to move less than one pixel during the time the target is scanned for a single frame. Thus unresolved targets only illuminate a single pixel per frame.

Nonscanned sensors are somewhat different because all pixels are collecting data during the entire frame time. The result is that in addition to the frame-to-frame motion expected for a moving target, the target moves within a frame, producing a streak or straight line within each frame. Thus a binary integration algorithm must sum over several pixels within each frame.

One approach to summing multiple pixels per frame is to implement the algorithm and architecture described above to account for the frame-to-frame motion, then combine outputs from the velocity filter to sum over multiple pixels per streak. This combining could be implemented in an ASIC, but is probably easier to implement in the CPU shown in Figure 23.

This algorithm is described by the following sequence. The basic idea is to form a one-dimensional output from the frame-to-frame portion of the velocity filter, which can then be convolved with a filter representing the moving target within a frame. The algorithm and architecture described earlier are used to obtain the one-dimensional data needed for the convolution.

1. Let u, v be the frame-to-frame movement in x, y for the desired velocity hypothesis, $u \geq 0$ and $v \geq 0$.
2. Let $\theta = \arctan(v/u)$ and $h = \sqrt{(u^2 + v^2)}$. The angle of the velocity vector is θ, and h is the length of that vector. The terms $\cos(\theta)$ and $\sin(\theta)$ may be computed here for later use.
3. Choose an initial point α, β for the integration, similar to i, j in the algorithm described in Section 2.3. In this case it is necessary to have either $\alpha = 0$ or $\beta = 0$, and $0 \leq \alpha \leq u$ and $0 \leq \beta \leq v$.
4. For $l = 0, \ldots, h-1$, do the following:
   (a) Let $i = \alpha + l\cos(\theta)$ and $j = \beta + l\sin(\theta)$.
   (b) Let the binary detection threshold be zero, $M = 0$.
   (c) Implement the algorithm described in Section 2.3, using the architecture in Figure 22 with the values of i, j and M specified above.
   (d) Outputs $s_{i+nu,j+nv}$ are saved according to: $f_{l+hn} = s_{i+nu,j+nv}$.
5. The one-dimensional data set f_n is an ordered sequence of outputs from convolving the frame-to-frame portion of the velocity filter with the data. The complete velocity filter output is computed by the convolution $f_n * g_n$, where $g_n = \{1, \ldots, 1\}$ is a sequence of h ones representing the target streak within a frame.
6. The output of the convolution is compared with the desired M-out-of-N detection threshold.

This algorithm may be viewed as postprocessing the result of the algorithm described in Sections 2.2 and 2.3. Postprocessing is a convolution by a rectangular window that can be implemented efficiently by sliding the window (adding one data point and subtracting another) without the need for an FFT approach.

3. CONCLUSION

A maximum likelihood moving target detection algorithm is derived based on a Gaussian model. Data samples are assumed to be temporally stationary, implying that image frames are registered and that there is no moving clutter. Data samples are allowed to be spatially nonstationary, corresponding to nonuniform background clutter.

In Section 1, the probability distribution of normalized experimental data is shown to agree closely with theoretical predictions. This agreement holds for a variety of clutter backgrounds (provided the temporal stationarity requirement is met) and validates studying the theoretical model as a means of predicting system performance, which is evaluated in terms of the probabilities of detection and false alarm.

In some system applications the computation and memory requirements of this algorithm may be large, particularly when either real-time processing or reduced processor size is required. A binary integration algorithm is developed in Section 2 to address these issues. Analyzing its detection and false alarm performance shows a 2-dB loss relative to the full-precision algorithm that is discussed in Section 1. Similar results are obtained in radar applications. To efficiently implement the binary integration algorithm an architecture concept is described that takes advantage of a small ASIC to perform the bulk of the computation.

One of many areas open for further research is frame registration; in many system applications the sensor is moving, requiring registration for sequential frames. Potential effects to be compensated include translation, scaling, and geometric distortion, and strongly depend on sensor design. Other registration issues arise due to moving (or apparently moving) clutter. In this case the entire frame is not adjusted; instead the clutter region must be selectively corrected. Difficulties arise along the edges of the moving clutter.

Another research area is incorporating target statistics models into the detection algorithm. The maximum likelihood algorithm described in Section 1 permits a single data sample of sufficient amplitude to cause a detection. An algorithm that requires a more distributed target signal component might offer improved performance.

Adapting the maximum likelihood algorithm to time-varying clutter backgrounds also requires further work. Not all backgrounds (e.g., sea glint) satisfy the temporal stationarity requirement.

APPENDIX A
MAXIMUM LIKELIHOOD ALGORITHM DERIVATION

A maximum likelihood algorithm (presented briefly in an earlier paper [3]) is developed for moving target detection. The following provides a more detailed derivation, using the model that (in the absence of targets) pixel samples are independent normal random variables that are temporally stationary. In other words, the underlying mean and variance of any given pixel is assumed constant from frame to frame. These means and variances are considered to be unknown and to vary spatially (i.e., from pixel to pixel).

This model is based on independent arrival of photons in each detector (a Poisson random variable approximated as normal). The average photon count in a given detector corresponds to the image intensity. The variance in the photon count is referred to as "photon noise." Additional sources are thermal and readout noise, which are also assumed to be independent from sample to sample.

Stationarity over time implies that all frames in a sequence are spatially registered and that there is no moving clutter. Nonstationary spatial statistics arise due to the nonuniform intensity of the background scene.

Prior to the algorithm derivation, it is useful to establish a notation that simplifies the equations. Unprocessed image data are represented by $r_{i,j,k}$, where (i,j) are the spatial indices and (k) is the temporal index. The set of indices that represent a given target motion hypothesis is denoted by S. It is assumed that the target moves a minimum of one pixel between frames. Set S contains M members with each member corresponding to a different pixel, (i,j).[5]

A simplified notation is used for the N frames of the M pixels in S. Pixel coordinates are mapped to a single sequential index. Additionally, the temporal index is permuted so that the hypothesized target is in those samples that have a temporal index of zero. To define this notation, let the pixels in S be represented by the triplet (i_m, j_m, k_m) for $0 \leq < M$. Data samples from these M pixels and N frames are represented by $\rho_{m,n}$, where

$$\rho_{m,n} = r_{i_m,j_m,l} \tag{A.1}$$

$$l = (n + k_m) \bmod N \tag{A.2}$$

and $0 \leq m < M$, $0 \leq n < N$.

---

[5]For a scanning sensor, an unresolved target occupies one pixel per frame, giving $M = N$. For a staring sensor, the target may move during the observation time and occupy several pixels per frame, giving $M > N$.

For the sample $\rho_{m,n}$, the unknown mean and variance of the noise are μ_m and σ_m^2, respectively. The unknown target component of $\rho_{m,0}$ is s_m.

The goal in this derivation is to develop a likelihood function to be tested in choosing between two hypotheses. Let H_1 be the hypothesis that a target is present, and let H_0 be the hypothesis that no target is present. The probability density of receiving data $\rho_{i,k}$, given hypothesis H_n, is

$$f_\rho(\{\rho_{i,k}\}|H_n) \quad . \tag{A.3}$$

The likelihood function, Λ, is defined as the ratio of this density for the two hypotheses, where the densities are maximized over the unknown parameters for clutter and signal [4].

$$\Lambda = \frac{\max_{\{\mu_i,\sigma_i,s_i\}} f_\rho(\{\rho_{i,k}\}|H_1)}{\max_{\{\mu_i,\sigma_i\}} f_\rho(\{\rho_{i,k}\}|H_0)} \tag{A.4}$$

The numerator is maximized over the set of μ_i, σ_i, and s_i for $0 \leq i < M$. Similarly, the denominator is maximized over the set of μ_i and σ_i for $0 \leq i < M$.

The maximization of the denominator is derived first. Because the $\rho_{i,k}$ are independent normal random variables, the density f_ρ is

$$f_\rho(\{\rho_{i,k}\}|H_0) = \prod_{i=0}^{M-1} \prod_{k=0}^{N-1} \frac{1}{\sqrt{2\pi\sigma_i^2}} \exp(-(\rho_{i,k} - \mu_i)^2/2\sigma_i^2) \quad . \tag{A.5}$$

Taking the partial derivative of this function with respect to the parameter μ_i gives

$$\frac{\partial}{\partial \mu_i} f_\rho = f_\rho \sum_{k=0}^{N-1} \frac{\rho_{i,k} - \mu_i}{\sigma_i^2} \quad , \tag{A.6}$$

where, for convenience, the argument to the function f_ρ is dropped. When this partial derivative is set to zero, it is seen that f_ρ is maximized when $\mu_i = a_i$, where

$$a_i = \frac{1}{N} \sum_{k=0}^{N-1} \rho_{i,k} \quad . \tag{A.7}$$

Similarly, substituting a_i for μ_i and taking the partial derivative of f_ρ with respect to the parameter σ_i^2 gives

$$\frac{\partial}{\partial \sigma_i^2} f_\rho = f_\rho \sum_{k=0}^{N-1} \frac{(\rho_{i,k} - a_i)^2 - \sigma_i^2}{2\sigma_i^4} \quad . \tag{A.8}$$

Setting Equation (A.8) to zero shows that f_ρ is maximized for $\sigma_i^2 = c_i$, where

$$c_i = \frac{1}{N} \sum_{k=0}^{N-1} (\rho_{i,k} - a_i)^2 \quad . \tag{A.9}$$

Finding the values of μ_i, σ_i, and s_i that maximize the numerator of Equation (A.4) is more complex. In this case the density f_ρ is given by

$$f_\rho(\{\rho_{i,k}\}|H_1) = \prod_{i=0}^{M-1} \prod_{k=0}^{N-1} \frac{1}{\sqrt{2\pi\sigma_i^2}} \exp(-(\rho_{i,k} - \mu_i - s_i\delta(k))^2/2\sigma_i^2) \quad , \tag{A.10}$$

where $\delta(k)$ is the Dirac delta function, defined to be unity for $k = 0$, and zero elsewhere. Taking the partial derivative of f_ρ with respect to these three parameters yields the following equations:

$$\frac{\partial}{\partial \mu_i} f_\rho = \left(\sum_{k=0}^{N-1} \frac{\rho_{i,k} - \mu_i}{\sigma_i^2} - \frac{s_i}{\sigma_i^2} \right) f_\rho \tag{A.11}$$

$$\frac{\partial}{\partial \sigma_i^2} f_\rho = \left(\frac{(\rho_{i,0} - \mu_i - s_i)^2 - \sigma_i^2}{2\sigma_i^4} + \sum_{k=1}^{N-1} \frac{(\rho_{i,k} - \mu_i)^2 - \sigma_i^2}{2\sigma_i^4} \right) f_\rho \tag{A.12}$$

$$\frac{\partial}{\partial s_i} f_\rho = \frac{\rho_{i,0} - \mu_i - s_i}{\sigma_i^2} f_\rho \quad . \tag{A.13}$$

Setting Equations (A.11), (A.12), and (A.13) to zero and solving the results simultaneously shows that f_ρ is maximized for

$$\mu_i = u_i \tag{A.14}$$

$$\sigma_i^2 = v_i \tag{A.15}$$

$$s_i = w_i \quad , \tag{A.16}$$

where

$$u_i = \frac{1}{N-1} \sum_{k=1}^{N-1} \rho_{i,k} \tag{A.17}$$

$$v_i = \frac{1}{N}\sum_{k=1}^{N-1}(\rho_{i,k} - u_i)^2 \tag{A.18}$$

$$w_i = \rho_{i,0} - u_i \quad . \tag{A.19}$$

Note that Equations (A.17) and (A.18) are different, particularly in the limits of the summations, from (A.7) and (A.9).

Substituting the density functions in Equations (A.5) and (A.10) into Equation (A.4) gives the following expression for the likelihood function when the numerator and denominator are maximized:

$$\Lambda = \frac{\prod_{i=0}^{M-1}\left[v^{-N/2}\prod_{k=1}^{N-1}\exp(-(\rho_{i,k}-u_i)^2/2v)\right]}{\prod_{i=0}^{M-1}\left[c^{-N/2}\prod_{k=0}^{N-1}\exp(-(\rho_{i,k}-a_i)^2/2c)\right]} \quad . \tag{A.20}$$

It is often easier to work with the logarithm of the likelihood function, which is

$$\mathcal{L} = \ln(\Lambda) \tag{A.21}$$

$$= \sum_{i=0}^{M-1}\left[\frac{-N}{2}\ln\left(\frac{v_i}{c_i}\right) - \sum_{k=1}^{N-1}\frac{(\rho_{i,k}-u_i)^2}{2v_i} + \sum_{k=0}^{N-1}\frac{(\rho_{i,k}-a_i)^2}{2c_i}\right] \quad . \tag{A.22}$$

This equation is simplified by first noting from Equations (A.9) and (A.18) that

$$\sum_{k=0}^{N-1}\frac{(\rho_{i,k}-a_i)^2}{2c_i} - \sum_{k=1}^{N-1}\frac{(\rho_{i,k}-u_i)^2}{2v_i} = 0 \quad . \tag{A.23}$$

Further simplification is obtained using the approximation

$$\ln(1+x) \approx x \tag{A.24}$$

for $|x| \ll 1$. The logarithm term in Equation (A.21) is then approximated by

$$\ln\left(\frac{v_i}{c_i}\right) = \ln\left(1 - \frac{1}{N-1}\frac{(\rho_{i,0}-a_i)^2}{c_i}\right) \tag{A.25}$$

$$\approx \frac{-1}{N-1}\frac{(\rho_{i,0}-a_i)^2}{c_i} \quad . \tag{A.26}$$

In evaluating the accuracy of this approximation, note that $\hat{s}_i^2 = (\rho_{i,0} - a_i)^2$ is an estimate of the target power in pixel i, and $\hat{\sigma}_i^2 = c_i$ is an estimate of the noise power. Thus the approximation is valid when the SNR is much smaller than the number of frames processed.[6] The resulting log-likelihood function is

$$\mathcal{L} = \frac{N}{2(N-1)} \sum_{i=0}^{M-1} \frac{(\rho_{i,0} - a_i)^2}{c_i} \quad . \tag{A.27}$$

The resulting maximum likelihood detection algorithm can now be stated as

$$H_1 \quad \text{if} \quad \mathcal{L} \geq t \tag{A.28}$$

$$H_0 \quad \text{if} \quad \mathcal{L} < t \quad , \tag{A.29}$$

where t is the detection threshold (often set for a constant false alarm rate criterion) and where, using the original notation $r_{i,j,k}$ for unprocessed data samples,

$$\mathcal{L} = \sum_{(i,j,k) \in S} d_{i,j,k} \tag{A.30}$$

$$d_{i,j,k} = \frac{(r_{i,j,k} - \hat{\mu}_{i,j})^2}{\hat{\sigma}_{i,j}^2} \tag{A.31}$$

$$\hat{\mu}_{i,j} = \frac{1}{N} \sum_{k=0}^{N-1} r_{i,j,k} \tag{A.32}$$

$$\hat{\sigma}_{i,j}^2 = \frac{1}{N} \sum_{k=0}^{N-1} (r_{i,j,k} - \hat{\mu}_{i,j})^2 \quad . \tag{A.33}$$

Set S is the set of spatial-temporal indices, (i,j,k), corresponding to the target motion hypothesis H_1. The constant multiplier in Equation (A.27) is dropped, noting that the constant can be incorporated into the detection threshold. The term $\hat{\mu}_{i,j}$ is the sample mean of N temporal samples of pixel (i,j). The term $\hat{\sigma}_{i,j}^2$ is the sample variance of the same N temporal samples of pixel (i,j).

---

[6] In the case where the SNR is not much smaller than the number of frames, the approximation to the log-likelihood function is less accurate. In such cases, however, the SNR is large and some loss can be tolerated.

The term $d_{i,j,k}$ is referred to as the "normalized" data. Finally, for this detection algorithm to be meaningful the number of frames processed must satisfy $N \geq 3$.

APPENDIX B
SINGLE PIXEL PROBABILITY DISTRIBUTIONS

The normalized data in the maximum likelihood electro-optic moving target detection algorithm is shown to have a beta distribution, which is used to determine the detection threshold, probability of false alarm, and probability of detection for both the full precision maximum likelihood detection and the binary integrator.

The log-likelihood function $\mathcal{L}$ of the maximum likelihood algorithm is expressed as the sum of normalized data $d_{i,j,k}$, where

$$\mathcal{L} = \sum_{(i,j,k)\in S} d_{i,j,k} \tag{B.1}$$

$$d_{i,j,k} = \frac{(r_{i,j,k} - \hat{\mu}_{i,j})^2}{\hat{\sigma}^2_{i,j}} \tag{B.2}$$

$$\hat{\mu}_{i,j} = \frac{1}{N}\sum_{n=0}^{N-1} r_{i,j,n} \tag{B.3}$$

$$\hat{\sigma}^2_{i,j} = \frac{1}{N}\sum_{n=0}^{N-1}(r_{i,j,n} - \hat{\mu}_{i,j})^2 \quad , \tag{B.4}$$

and S is the set of space (i,j) and time (k) indices corresponding to the target motion hypothesis.

The probability distribution $F_d(x|N)$ of $d_{i,j,k}$ is shown to follow a beta distribution for the noise-only case and a noncentral beta distribution when a target is present. For the radar case, where μ is known a priori to be zero and where $r_{i,j,k}$ is complex, this distribution is well known [5].

B.1 Distribution for Noise Only (No Target)

The direction taken is to relate the distribution $F_d(x|N)$ of $d_{i,j,k}$ to the beta distribution. For notational simplicity, the pixel indices (i,j) will be dropped because they never change during the derivation.

The beta probability density function (pdf) with parameters α and β is

$$f_B(x|\alpha,\beta) = \frac{\Gamma(\alpha+\beta)}{\Gamma(\alpha)\Gamma(\beta)} x^{\alpha-1}(1-x)^{\beta-1} \tag{B.5}$$

for $0 < x < 1$, and $f_B(x|\alpha,\beta) = 0$ elsewhere. If X_1 and X_2 are independent chi-square random variables with ν_1 and ν_2 degrees of freedom respectively, then the ratio

$$\frac{X_1}{X_1 + X_2} \tag{B.6}$$

has the beta distribution

$$F_B\left(x \middle| \frac{\nu_1}{2}, \frac{\nu_2}{2}\right) \quad . \tag{B.7}$$

The random variable d_k can be written in a form similar to Equation (B.6) by using a linear transformation of independent random variables. Let Q be an orthogonal $N \times N$ matrix, and let $\underline{u}$ be a length-N vector of independent standard normal random variables (i.e., zero mean and unity variance), where the nth element is

$$u_n = \frac{r_n - \mu}{\sigma} \tag{B.8}$$

for $0 \leq n < N$. Then the vector

$$\underline{v} = Q\underline{u} \tag{B.9}$$

is also a vector of independent standard normal random variables v_n, where $0 \leq n < N$.

Many possible orthogonal matrices can be constructed. Let the first and second rows of Q be

$$\left[\frac{1}{\sqrt{N}}, \ldots, \frac{1}{\sqrt{N}}\right] \tag{B.10}$$

and

$$\left(\underline{e}_k - \left[\frac{1}{N}, \ldots, \frac{1}{N}\right]\right)\sqrt{\frac{N}{N-1}} \quad , \tag{B.11}$$

where $\underline{e}_k$ is a vector with a one in the kth position and zeros elsewhere. It is easy to verify that these two rows are orthogonal, and each has unity norm as is necessary for Q to be orthogonal.

Let $\bar{u}$ represent the sample average of the u_n,

$$\bar{u} = \frac{1}{N}\sum_{n=0}^{N-1} u_n \quad . \tag{B.12}$$

It is easy to show that

$$v_0 = \bar{u}\sqrt{N} \tag{B.13}$$

$$v_1 = (r_k - \hat{\mu})\frac{1}{\sigma}\sqrt{\frac{N}{N-1}} \tag{B.14}$$

$$\sum_{n=0}^{N-1} v_n^2 = \sum_{n=0}^{N-1} u_n^2 \quad . \tag{B.15}$$

The transformation of independent standard normal random variables is next used to derive the distribution of d_k. Note that $(r_k - \hat{\mu})$ is related to u_n by

$$(r_n - \hat{\mu}) = (u_n - \bar{u})\sigma \quad . \tag{B.16}$$

This equality, along with Equations (B.13) and (B.15), is used to give the following relation between the denominator in the definition of d_k in Equation (B.2) and the v_n:

$$\begin{aligned} \sum_{n=0}^{N-1}(r_n - \hat{\mu})^2 &= \sigma^2 \sum_{n=0}^{N-1}(u_n - \bar{u})^2 \\ &= \sigma^2 \left(-N\bar{u}^2 + \sum_{n=0}^{N-1} u_n^2\right) \\ &= \sigma^2 \sum_{n=1}^{N-1} v_n^2 \quad . \end{aligned} \tag{B.17}$$

Combining Equations (B.2), (B.4), (B.14), and (B.17) gives the following representation for d_k:

$$d_k = \frac{(r_k - \hat{\mu})^2}{\sum_{n=0}^{N-1}(r_n - \hat{\mu})^2} N \tag{B.18}$$

$$= \frac{v_1^2}{v_1^2 + \sum_{n=2}^{N-1} v_n^2}(N-1) \quad . \tag{B.19}$$

Because the v_n are independent and have standard normal distribution, the term v_1^2 is chi-square with one degree of freedom, and $\sum_{n=2}^{N-1} v_n^2$ is chi-square with $N-2$ degrees of freedom. Referring to Equation (B.6), it is clear that d_k has the beta distribution

$$F_d(x|N) = F_B\left(\frac{x}{N-1}\middle|\frac{1}{2}, \frac{N-2}{2}\right) \quad , \tag{B.20}$$

where

$$0 \leq x \leq N-1 \quad . \tag{B.21}$$

B.2 Distribution with Target

The probability distribution of a normalized pixel with a target present is shown to be a noncentral beta distribution. In this case the chi-square random variable in the numerator of Equation (B.6) is derived from normal distributed random variables with nonzero means. As in Section B.1, a linear transformation is applied to the data to obtain the desired form.

Let s be the target component of the data sample r_k, and define $\underline{u}$ to be a length N vector formed from the data samples, where

$$u_n = \frac{r_n - \mu - \frac{1}{N}s}{\sigma} \quad . \tag{B.22}$$

These u_n are independent normal random variables with unity variance and nonzero mean.

Let Q be the orthogonal matrix defined in Section B.1. Then the vector

$$\underline{v} = Q\underline{u} \tag{B.23}$$

is also a vector of independent normal random variables with unity variance and nonzero mean. The derivation outlined in Equations (B.12) through (B.19) is repeated to show again that

$$d_k = \frac{v_1^2}{v_1^2 + \sum_{n=2}^{N-1} v_n^2}(N-1) \quad . \tag{B.24}$$

It will be shown that v_1 is a noncentral chi-square random variable with one degree of freedom, and $\sum_{n=2}^{N-1} v_n$ is a central chi-square random variable with $N-2$ degrees of freedom. The normalized data d_k then have a noncentral beta distribution.

From Equations (B.13) and (B.14), the means of the random variables v_0 and v_1 are

$$E\{v_0\} = 0 \tag{B.25}$$

$$E\{v_1\} = \frac{s}{\sigma}\sqrt{\frac{N-1}{N}} \quad . \tag{B.26}$$

The means of the remaining v_n are shown to be zero by evaluating the sum of the squares of the means of the v_n, using Equations (B.25) and (B.26).

$$\sum_{n=1}^{N-1} E\{v_n\}^2 = \sum_{n=0}^{N-1} E\{v_n\}^2 \tag{B.27}$$

$$= \sum_{n=0}^{N-1} E\{u_n\}^2 \tag{B.28}$$

$$= \frac{s^2}{\sigma^2}\frac{N-1}{N} \tag{B.29}$$

$$= E\{v_1\}^2 \tag{B.30}$$

Subtracting $E\{v_1\}^2$ from both sides of Equation (B.30) proves that only v_1 has nonzero mean. Thus Equation (B.24) indicates that d_k has the noncentral beta distribution given by

$$F_d(x|N,\lambda) = F_{B'}\left(\frac{x}{N-1}\middle|\frac{1}{2},\frac{N-2}{2},\lambda\right) \quad , \tag{B.31}$$

where

$$0 \le x \le N-1 \quad , \tag{B.32}$$

and λ is the noncentrality parameter

$$\lambda = \frac{s^2}{\sigma^2}\frac{N-1}{N} \quad . \tag{B.33}$$

The noncentral beta distribution can be written in terms of the central beta distribution according to

$$F_{B'}(x|\alpha,\beta,\lambda) = \sum_{n=0}^{\infty} e^{-\lambda/2}\frac{(\lambda/2)^n}{n!}F_B(x|\alpha+n,\beta) \quad . \tag{B.34}$$

This formula is easily derived from one that is similar for the noncentral F distribution ([6], p. 192).

It is interesting to note that for a given number of image frames N, the noncentrality parameter λ is the product of a constant with the signal-power to noise-power ratio s^2/σ^2, which is referred to as an "instantaneous" signal-to-noise ratio, $\mathrm{SNR_i}$. A similar dependency occurs for many other detection problems. When the signal power is zero, the noncentral distribution in Equation (B.34) reduces to a single central beta distribution, as it should.

APPENDIX C
LIKELIHOOD FUNCTION STATISTICS

The probability distribution of the log-likelihood function is needed to determine the probabilities of detection and false alarm for the maximum likelihood algorithm and is expressed in terms of the density function derived in Appendix B for normalized pixels.

The log-likelihood function probability distribution $F_{\mathcal{L}}(x)$ depends on the SNR through the parameter $\lambda = \frac{N-1}{N}\mathrm{SNR_i}$ in the single pixel distribution function, $F_d(x|N,\lambda)$. In computing the probability of false alarm, the $\mathrm{SNR_i}$ is zero. In computing the probability of detection, the statistical distribution of $\mathrm{SNR_i}$ should be taken into account in computing $F_{\mathcal{L}}(x)$. The distribution of $\mathrm{SNR_i}$ depends on the statistics of receiving target photons as well as those of background clutter intensity. The approach taken here is to compute $F_d(x|N,\lambda)$ for constant $\mathrm{SNR_i}$. The results are useful in discussing target detection in terms of an effective signal-to-noise ratio, $\mathrm{SNR_{eff}}$, as described at the end of Section 1.4.

The log-likelihood function $\mathcal{L}$ is the sum of normalized data $d_{i,j,k}$:

$$\mathcal{L} = \sum_{(i,j,k)\in S} d_{i,j,k} \quad , \tag{C.1}$$

where S is the set of coordinates for the target velocity hypothesis. The model used in the maximum likelihood derivation in Appendix A implies that $d_{i,j,k}$ are independent random variables; therefore, the density function $f_{\mathcal{L}}(x)$ of $\mathcal{L}$ is the convolution of the densities of $d_{i,j,k}$. The single pixel density function is obtained by differentiating Equation (B.31) with respect to x, yielding

$$f_d(x|N,\lambda) = \frac{1}{N-1} f_{B'}\left(\frac{x}{N-1}\middle|\frac{1}{2},\frac{N-2}{2},\lambda\right) \quad , \tag{C.2}$$

where $f_{B'}$ is the noncentral beta density.

Let M be the number of elements in the set S (i.e., M is the number of samples in the target motion hypothesis). The log-likelihood density function is then obtained as the convolution of M density functions,

$$f_{\mathcal{L}}(x|N,\lambda) = f_d * \cdots * f_d(x|N,\lambda) \quad . \tag{C.3}$$

The distribution function is the integral of the density function, which can also be expressed as a convolution of density functions with a unit step function, $h(x)$,

$$F_{\mathcal{L}}(x|N,\lambda) = \int_{-\infty}^{x} f_{\mathcal{L}}(u|N,\lambda)\, du \tag{C.4}$$

$$= h * f_{\mathcal{L}}(x|N,\lambda) \tag{C.5}$$

$$= h * f_d * \cdots * f_d(x|N,\lambda) \quad , \tag{C.6}$$

where

$$h(x) = \begin{cases} 0, & x < 0 \\ 1, & x \geq 0 \end{cases} \quad . \tag{C.7}$$

The probabilities of detection and false alarm are the complement, $1 - F_{\mathcal{L}}(x|N,\lambda)$, of the distribution function and may be expressed as the convolutions

$$P_D(x|N,\lambda) = (1-h) * f_d * \cdots * f_d(x|N,\lambda) \tag{C.8}$$

$$P_{FA}(x|N) = (1-h) * f_d * \cdots * f_d(x|N,\lambda=0) \quad , \tag{C.9}$$

where x is the detection threshold. Simple formulas for these probabilities are difficult to obtain. Convolutions can, however, be evaluated through numerical integration; the remainder of this appendix discusses the details. Results are plotted in Figure 11 where $N = 10$-frame processing for a scanning sensor (i.e., $M = N$).

The M-fold convolution in Equation (C.8) can be computed as an Mth order integral. The difficulty in such an integration is maintaining accuracy while computing numerical results in a reasonable time. The approach taken for each convolution is to sample the function to be integrated at uniform intervals along the x-axis and use Simpson's rule [7, 8] to compute the resulting convolution at these same sample points. This approach is applied M times in succession to obtain the final convolution.

The first convolution in Equation (C.8) is easily shown to be

$$(1-h) * f_d(x|N,\lambda) = 1 - F_d(x|N,\lambda) \tag{C.10}$$

$$= F_{B'}\left(1 - \frac{x}{N-1} \middle| \frac{N-2}{2}, \frac{1}{2}, \lambda\right) \tag{C.11}$$

and can be computed without using numerical integration. This function, and each subsequent convolution of $f_d(x|N,\lambda)$ with this function, is the complement of a probability distribution.

Let K, a positive even number, be the number of sample intervals in the range $0 \leq x \leq N-1$, and let δ be the sample interval,

$$\delta = \frac{N-1}{K} \quad . \tag{C.12}$$

For $N > 3$ the convolutions are computed by first defining two sample sequences, g_n and $u_n^{(1)}$, where

$$g_n = \begin{cases} f_d(\gamma\delta|N,\lambda), & n = 0 \\ f_d(n\delta|N,\lambda), & n = 1,\ldots,K \\ 0, & n > K \end{cases} \tag{C.13}$$

$$u_n^{(1)} = \begin{cases} 1, & n \le 0 \\ F_{B'}\left(1 - \frac{n\delta}{N-1}\left|\frac{N-2}{2},\frac{1}{2},\lambda\right.\right), & n = 1,\ldots,K \\ 0, & n > K \end{cases} . \tag{C.14}$$

The superscript (m) on $u_n^{(m)}$ indicates the number of convolutions represented by the sequence. Convolutions are computed using g_n and $u_n^{(m)}$ to produce $u_n^{(m+1)}$.

The parameter γ is carefully chosen in the range $0 < \gamma < 1$ to avoid a singularity in $f_d(x|N,\lambda)$. [For $N = 3$ the density $f_d(x|N,\lambda)$ also has a singularity at $x = 2$.] As x approaches zero from above, this function approaches infinity. The parameter γ is chosen so that when Simpson's rule is applied directly to the sequence g_n, representing an approximation to integrating the density function $f_d(x|N,\lambda)$, the result is very close to unity. For example, with $N = 10$, $\lambda = 0$, $K = 1{,}000$, and $\gamma = 0.0701267113512541$, the result of applying Simpson's rule to g_n is $1 + \epsilon$, where $|\epsilon| < 10^{-16}$.

Higher order convolutions are computed according to the formula

$$u_k^{(m+1)} = \begin{cases} 1, & k \le 0 \\ \frac{\delta}{3}\sum_{n=k-K}^{\min(mK,k)} w_{n-k+K}\, u_n^{(m)} g_{k-n}, & k = 1,\ldots,(m+1)K \\ 0, & k > (m+1)K \end{cases} \tag{C.15}$$

for $m = 1,\ldots,M-1$, and where the weighting sequence w_n used in Simpson's rule is given by

$\min(mK,k) - (k-K)$	$w_0,\ldots,w_{\min(mK,k)-(k-K)}$
0	$\{1\}$
1	$\{4,1\}$
even	$\{1,4,2,4,\ldots,4,2,4,1\}$
odd	$\{4,2,4,\ldots,4,2,4,1\}$

(C.16)

Simpson's rule requires an even number of sampling intervals (or an odd number of sampling points). In the case where the number of intervals, $\min(mK, k) - (k - K)$, is odd, the additional term

$$w_{-1} u^{(m)}_{k-K-1} g_{K+1} \tag{C.17}$$

can be added to the summation in Equation (C.15) for $w_{-1} = 1$; however, $g_{K+1} = 0$ and $0 \leq u^{(m)}_{k-K-1} \leq 1$ so that this additional term is known to be zero and can be omitted from the summation. Accuracy of the result when use of this additional term is implied is ensured by noting that $u^{(m)}_n$ represents samples of a continuous function for all n, and g_n represents samples of a continuous function for $n \geq 1$ (when $N > 3$).

The probability of detection is approximated by

$$P_D(n\delta | N, \lambda) \approx u^{(M)}_n \quad . \tag{C.18}$$

The probability of false alarm is obtained with the same formula for the case $\lambda = 0$.

REFERENCES

1. M.I. Skolnik, *Radar Handbook*, New York: McGraw-Hill (1990).
2. D.K. Barton, *Radar System Analysis*, Dedham, Mass.: Artech House (1986).
3. A.E. Filip, "Processor Technology for Visible Band, Electro-Optical Sensors," *Proc. AIAA Computers in Aerospace VII Conference*, Monterey, Calif. (1989), pp. 320–325.
4. M.H. DeGroot, *Probability and Statistics*, Reading, Mass.: Addison-Wesley (1975).
5. E.J. Kelly and K.M. Forsythe, "Adaptive Detection and Parameter Estimation for Multidimensional Signal Models," MIT Lincoln Laboratory, Lexington Mass., Technical Rep. 848 (19 April 1989), DTIC AD-A208971.
6. N.L. Johnson and S. Kotz, *Distributions in Statistics: Continuous Univariate Distributions—2*, New York: Wiley (1970).
7. W.H. Beyer, *Handbook of Mathematic Sciences*, Boca Raton, Fla.: CRC Press, Inc. (1978).
8. L. Fox and D.E. Mayers, *Computing Methods for Scientists and Engineers*, London: Oxford University Press (1968).

REPORT DOCUMENTATION PAGE

Form Approved
OMB No. 0704-0188

1. AGENCY USE ONLY (*Leave blank*)	2. REPORT DATE	3. REPORT TYPE AND DATES COVERED
	16 January 1992	Technical Report

4. TITLE AND SUBTITLE

Maximum Likelihood Detection of Electro-optic Moving Targets

5. FUNDING NUMBERS

C — F19628-90-C-0002
PE — 63003F, 63226E/63214C
PR — 331/773

6. AUTHOR(S)

Stephen C. Pohlig

7. PERFORMING ORGANIZATION NAME(S) AND ADDRESS(ES)

Lincoln Laboratory, MIT
P.O. Box 73
Lexington, MA 02173-9108

8. PERFORMING ORGANIZATION REPORT NUMBER

TR-940

9. SPONSORING/MONITORING AGENCY NAME(S) AND ADDRESS(ES)

HQ AF Space Systems Division
Los Angeles AFB, CA 90009-2960

10. SPONSORING/MONITORING AGENCY REPORT NUMBER

ESD-TR-91-174

11. SUPPLEMENTARY NOTES

None

12a. DISTRIBUTION/AVAILABILITY STATEMENT

Approved for public release; distribution is unlimited.

12b. DISTRIBUTION CODE

13. ABSTRACT (*Maximum 200 words*)

The description of a maximum likelihood algorithm to detect moving targets in electro-optic data is presented. The algorithm is based on processing image data that are modeled as temporally stationary and spatially nonstationary Gaussian samples. Algorithm performance is evaluated in terms of the probabilities of false alarm and detection. A comparison of theoretical and experimental probability distributions for single normalized pixels shows good agreement for different clutter backgrounds (stellar, sky, mountains, and desert). Similarly, a comparison of theoretical and experimental false alarm probabilities also shows good agreement. These results validate using theoretical models to predict performance.

A binary integration version of this algorithm is described and evaluated in terms of false alarm and detection probabilities. This version is suboptimum and is compared with the optimum algorithm to determine the performance loss. A processing architecture concept is also described.

14. SUBJECT TERMS		15. NUMBER OF PAGES
maximum likelihood	electro-optic sensor	68
detection	infrared sensor	16. PRICE CODE
moving target	binary integration	
velocity filter		

17. SECURITY CLASSIFICATION OF REPORT	18. SECURITY CLASSIFICATION OF THIS PAGE	19. SECURITY CLASSIFICATION OF ABSTRACT	20. LIMITATION OF ABSTRACT
Unclassified	Unclassified	Unclassified	SAR